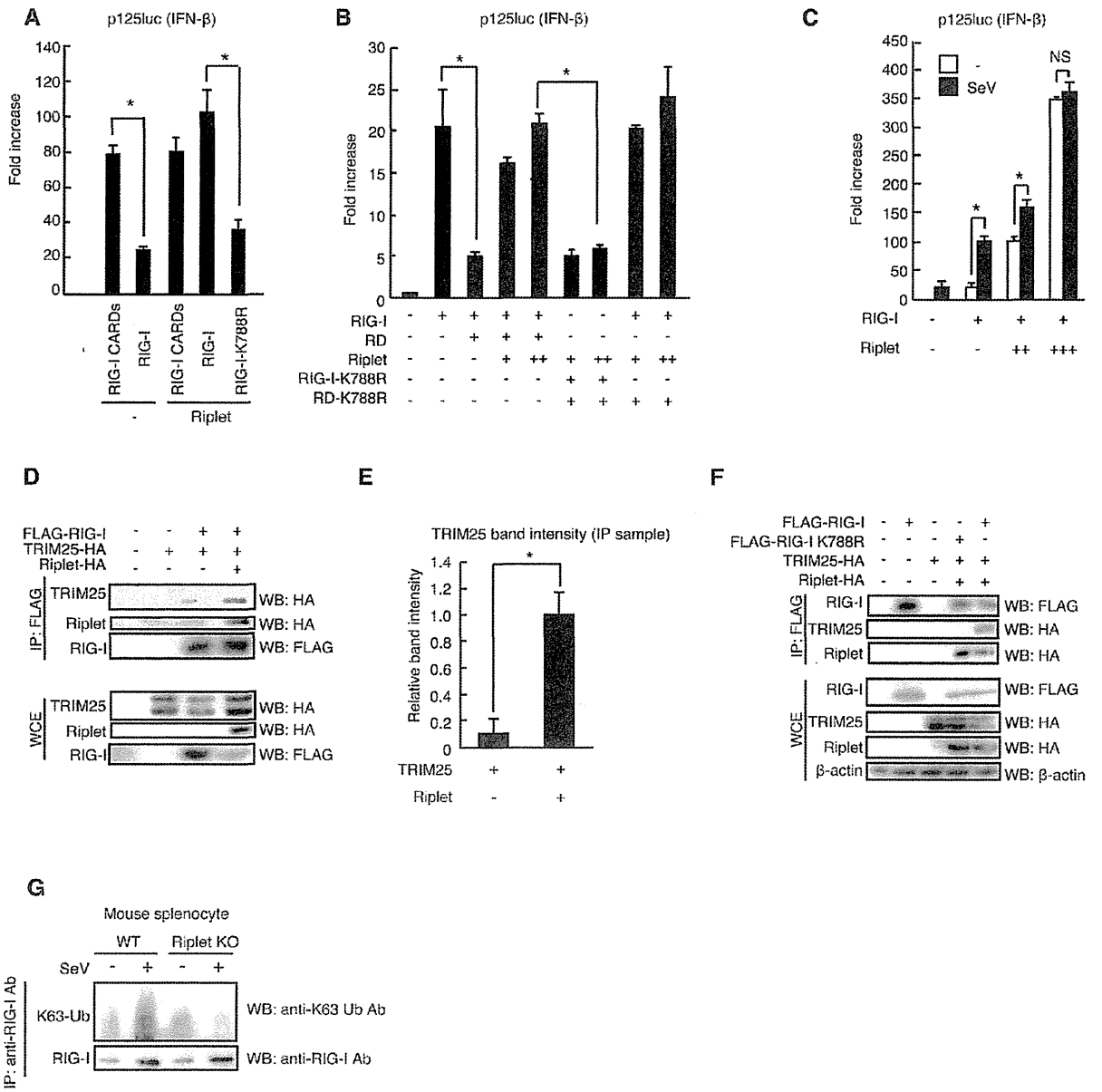

Figure 5. Riplet affects RIG-I RD autorepression of CARDs signaling. (A, B) IFN-β promoter activation was determined using a p125luc IFN-β reporter gene. Expression vectors encoding RIG-I CARDs, full-length RIG-I, RIG-I K788R, RD, RD-K788, and/or Riplet were transfected into HEK293 cells as indicated. Reporter activation was determined after transfection. Data are presented as mean ± SD (n = 3). *$p<0.05$. (C) IFN-β promoter activation was determined using a p125luc IFN-β reporter gene. RIG-I and Riplet expression vectors were transfected into HEK293 cells as indicated. 24 hours after transfection, cells were infected with SeV at MOI = 1 for 24 hours, and the reporter activities were determined. (D–F) HEK293FT cells were transfected with expression vectors encoding FLAG-tagged RIG-I, HA-tagged TRIM25, HA-tagged Riplet, FLAG-tagged RIG-I K788R as indicated. Cell lysate was prepared at 24 hours after transfection, followed by immunoprecipitation with an anti-FLAG antibody (RIG-I). Relative band intensity of immunoprecipitated TRIM25 in panel D was determined (E). (G) Mouse splenocyte was isolated from wild-type and Riplet KO mice spleen. The cells were infected with SeV, and then cell lysate was prepared. Immunoprecipitation was carried out with anti-RIG-I rabbit mAb (D14G6), and subjected to SDS-PAGE. Endogenous K63-linked polyubiquitin chain was detected using K63-linked polyubiquitin chain specific antibody.
doi:10.1371/journal.ppat.1003533.g005

HCV RNA (Figure 9E) but not in HuH7.5 cell line (Figure 9E). In HuH7.5 cells, there is a T55I mutation within endogenous *RIG-I* gene that disrupts the interaction between RIG-I and TRIM25 [38]. We investigated whether Riplet is required for RIG-I to exhibit punctate staining, and found that knockdown of Riplet decreased RIG-I punctate staining induced by HCV RNA (Supplemental Figure S4). We next investigated whether HCV abrogated Riplet-dependent RIG-I punctate pattern in the cytoplasm. As expected, RIG-I failed to exhibit punctate staining in O cells with HCV replicons in NS3 positive cells and HuH7

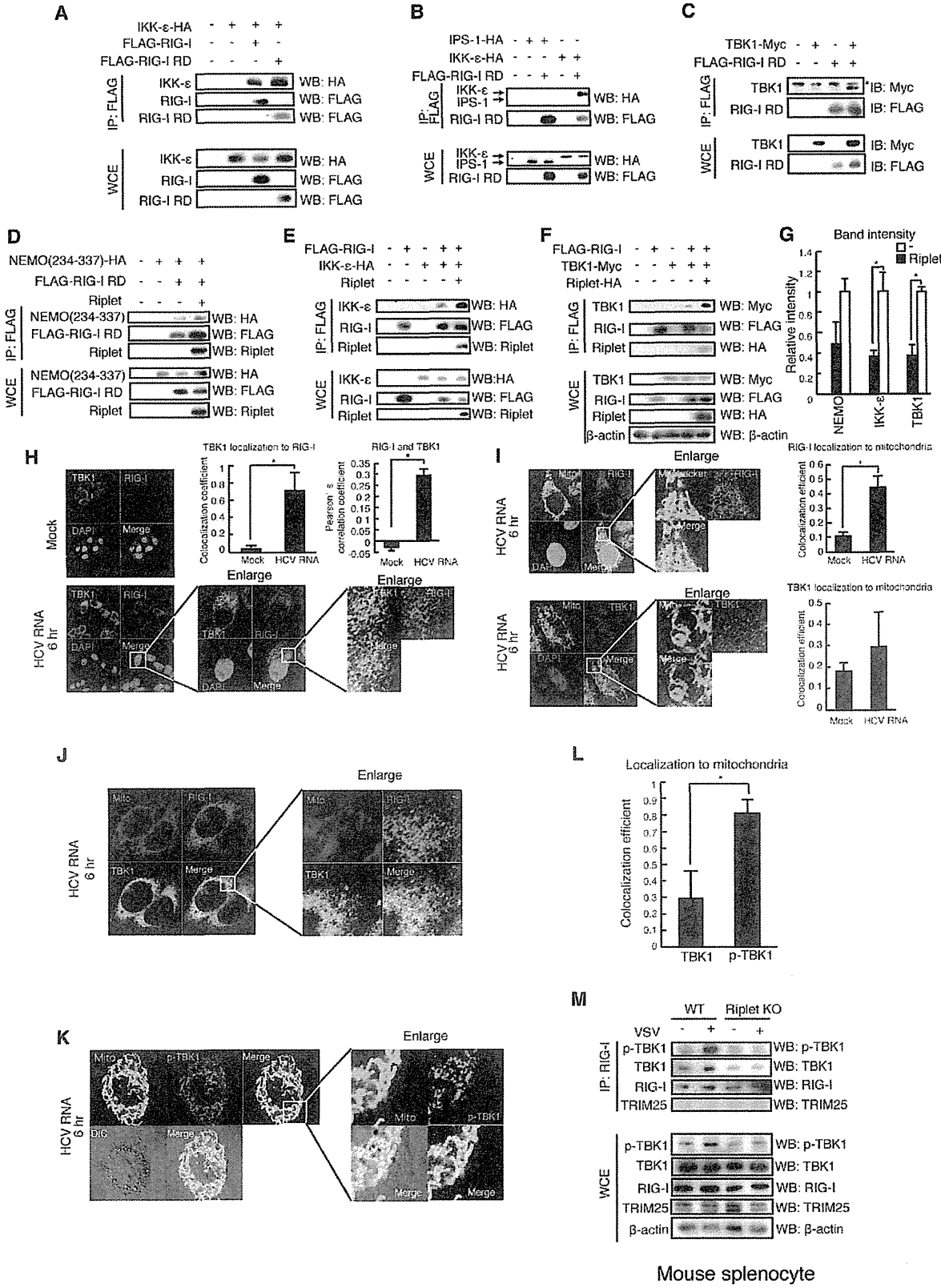
A
IKK-ε-HA
FLAG-RIG-I
FLAG-RIG-I RD
IP: FLAG
IKK-ε
RIG-I
RIG-I RD
WB: HA
WB: FLAG
WCE
B
IPS-1-HA
IKK-ε-HA
FLAG-RIG-I RD
IKK-ε
IPS-1
RIG-I RD
C
TBK1-Myc
FLAG-RIG-I RD
TBK1
IB: Myc
IB: FLAG
D
NEMO(234-337)-HA
Riplet
NEMO(234-337)
WB: Riplet
E
F
TBK1-Myc
Riplet-HA
TBK1
WB: Myc
β-actin
WB: β-actin
G
Band intensity
Riplet
Relative intensity
NEMO
IKK-ε
TBK1
H
TBK1 localization to RIG-I
RIG-I and TBK1
Mock
HCV RNA 6 hr
Enlarge
Colocalization coefficient
Pearson's correlation coefficient
I
RIG-I localization to mitochondria
Colocalization efficient
J
K
L
Localization to mitochondria
TBK1
p-TBK1
M
WT
Riplet KO
VSV
WB: p-TBK1
WB: TBK1
WB: RIG-I
WB: TRIM25
Mouse splenocyte

Figure 6. The association of TBK1 and IKK-ε protein kinases with RIG-I RD is enhanced by Riplet. (A–F) The interaction of RIG-I with TBK1, IKK-ε, and NEMO was examined by immunoprecipitation assay. FLAG-tagged RIG-I or RIG-I RD expression vector was transfected into HEK293FT cells together with HA-tagged IKK-ε (A, B, and E), Myc-tagged TBK1 (C, F), HA-tagged NEMO ubiquitin binding region (D), and/or Riplet (D–F) expression vectors as indicated. 24 hours after the transfection, cell lysate was prepared, and immunoprecipitation was performed with anti-FLAG antibody. Asterisk indicates non-specific bands. (G) Relative band intensity of immunoprecipitated NEMO, IKK-ε, and TBK1 in D–F was determined. (H–L) Intracellular localization of endogenous RIG-I (H–J), TBK1 (H–J), phosphorylated-TBK1 (p-TBK1) (K), and mitochondria (I–K) were observed using anti-RIG-I (Alme-1), TBK1, p-TBK1 mAbs, and mitotracker. HeLa cells were stimulated with HCV dsRNA for six hours using lipofectamine 2000. Colocalization coefficient of TBK1 localization to RIG-I (H), RIG-I and TBK1 localization to mitochondria (I), and TBK1 and p-TBK1 localization to mitochondria (L) were determined (mean ± sd, n>10). Person's correlation coefficient of RIG-I and TBK1 was determined (H). (M) Splenocytes from wild type and Riplet KO mouse were infected with VSV at MOI = 10 for eight hours. Immunoprecipitation was performed using an anti-RIG-I rabbit monoclonal antibody (D14G6), and the immunoprecipitates were analyzed by SDS-PAGE. Endogenous RIG-I, TBK1, TRIM25, and β-actin were detected using anti-RIG-I, p-TBK1, TRIM25, and β-actin antibodies.
doi:10.1371/journal.ppat.1003533.g006

cells infected with HCV JFH1 (Figure 9F–9H). We confirmed that HCV disrupted IPS-1 in our experimental condition (Figure 9G and 9H).

To further assess whether HCV abrogates endogenous Riplet function, we observed endogenous K63-linked polyubiquitination of RIG-I in cells with HCV replicons. Although SeV infection induced endogenous K63-linked polyubiquitination of RIG-I in HuH7 cells, HCV replicons failed to increase the polyubiquitination (Figure 9I). Next, we investigated the association of endogenous RIG-I with TRIM25 and TBK1, which is promoted by Riplet as shown in Figure 5 and 6. SeV infection induced the association of endogenous RIG-I with TRIM25 and TBK1, whereas HCV replicons failed to induce the association (Figure 9J). Taken together, these data indicated that HCV abrogated endogenous Riplet function.

Although NS3-4A cleaves IPS-1, a mutation within endogenous *RIG-I* gene increased the permissiveness to HCV infection in HuH7-derived cells [3], indicating that RIG-I is required for antiviral response to HCV infection before NS3-4A cleaves IPS-1. We used siRNA to knockdown endogenous Riplet in HuH7 cells, and then the cells were infected with HCV JFH1. Interestingly, Riplet knockdown increased the permissiveness to HCV JFH1 infection (Figure 9K), indicating that endogenous Riplet is required for antiviral response to HCV infection.

Discussion

RIG-I activation is regulated by two ubiquitin ligases Riplet and TRIM25 [15,21]. The two ubiquitin ligases are essential for RIG-I activation [15,23], however the functional difference had been unclear. It is known that TRIM25 is essential for RIG-I oligomerization and association with IPS-1 adaptor molecule [15,19]. Here, we demonstrated that Riplet was essential for the release of RIG-I RD autorepression of its CARDs, which resulted in the association with TRIM25. This functional difference explained the reason why RIG-I requires the two ubiquitin ligases for triggering the signal.

It has been reported that TRIM25 activates RIG-I signaling [15,19]. We confirmed that ectopic expression of TRIM25 increases RIG-I CARDs-mediated signaling. However, most previous studies used a RIG-I CARDs fragment but not full-length RIG-I [15,19,38]. Unexpectedly, we found that the increase of full-length RIG-I-mediated signaling by TRIM25 expression was much less than that of the CARDs-mediated signaling. It is intriguing that Riplet helped TRIM25 to activate full-length RIG-I. Riplet expression promoted the interaction between TRIM25 and full-length RIG-I, and this interaction was abrogated by an RIG-I K788R mutation, which reduced Riplet-mediated RIG-I ubiquitination. Thus, we propose that Riplet-mediated polyubiquitination of RIG-I RD is a prerequisite for TRIM25 to activate RIG-I (Figure 10).

Ectopic expression of Riplet activated RIG-I without stimulation with RIG-I ligand. This is not surprising because ectopically expressed Riplet bound to RIG-I without stimulation with RIG-I ligand, whereas endogenous Riplet bound to endogenous RIG-I after stimulation with RIG-I ligand. RIG-I undergoes its conformational change after binding to a ligand [3,39]. The conformational change would allow the access of endogenous Riplet to RIG-I, which resulted in Riplet-mediated K63-linked polyubiquitination leading to the release of RD autorepression. This model is consistent with the observation that TRIM25 ectopic expression did not activate full-length RIG-I without Riplet expression, because TRIM25 hardly bound to full-length RIG-I without Riplet.

Previously, we reported that the five Lys residues within RIG-I RD were important for Riplet-mediated RIG-I ubiquitination. We constructed the RIG-I 5KR mutant and indicated that the 5KR mutation reduced RIG-I ubiquitination and activation without loss of RNA binding activity. This is consistent with our previous conclusion. However, there is residual ubiquitination of RIG-I 5KR mutation, and we found that K788R mutation showed more sever phenotype. These data indicated that Riplet targeted the several Lys residues within RIG-I RD. This is not surprising, because TRIM25 targets not only Lys-172 but also other Lys residues within mouse RIG-I CARDs [32].

TBK1 and IKK-ε are downstream factors of IPS-1. We found that TBK1 and IKK-ε could bind RIG-I RD. It is possible that RIG-I associates with TBK1 through IPS-1. However, Hiscott J and colleagues demonstrated that IKK-ε could bind IPS-1 and that TBK1 did not bind IPS-1 [40]. Moreover, RIG-I RD did not bind IPS-1, and RIG-I and TBK1 co-localization was detected in the cytoplasmic region where there are no mitochondria. These observations weaken this possibility. Our results indicated that RIG-I RD bound to the NEMO ubiquitin binding region. IRF-3 activation requires the ubiquitin binding domain of NEMO, and an endogenous K63-linked polyubiquitin chain plays a key role in IRF3 activation [41]. Thus, we prefer a model in which TBK1 associates with an RIG-I RD-anchored polyubiquitin chain through NEMO (Figure 10). Although Riplet knockout reduced the binding of RIG-I to TBK1, residual binding was still detectable. Thus, there appears to be Riplet-dependent and independent associations between RIG-I and TBK1. TRAF3 is an E3 ubiquitin ligase, and is involved in the RIG-I-mediated type I IFN production pathway [42]. Because there is residual activation of the type I IFN production pathway even in TRAF3 knockout cells [41], it is possible that the RIG-I polyubiquitin chain may compensate for the TRAF3 defect in recruiting TBK1 to mitochondria. Further studies will be needed to determine the precise molecular mechanisms. Although TBK1 dispersed in the cytoplasm, p-TBK1 was exclusively localized on mitochondria. Considering that TBK1 is phosphorylated in its activation loop [33], these results suggested that RIG-I RD associated with

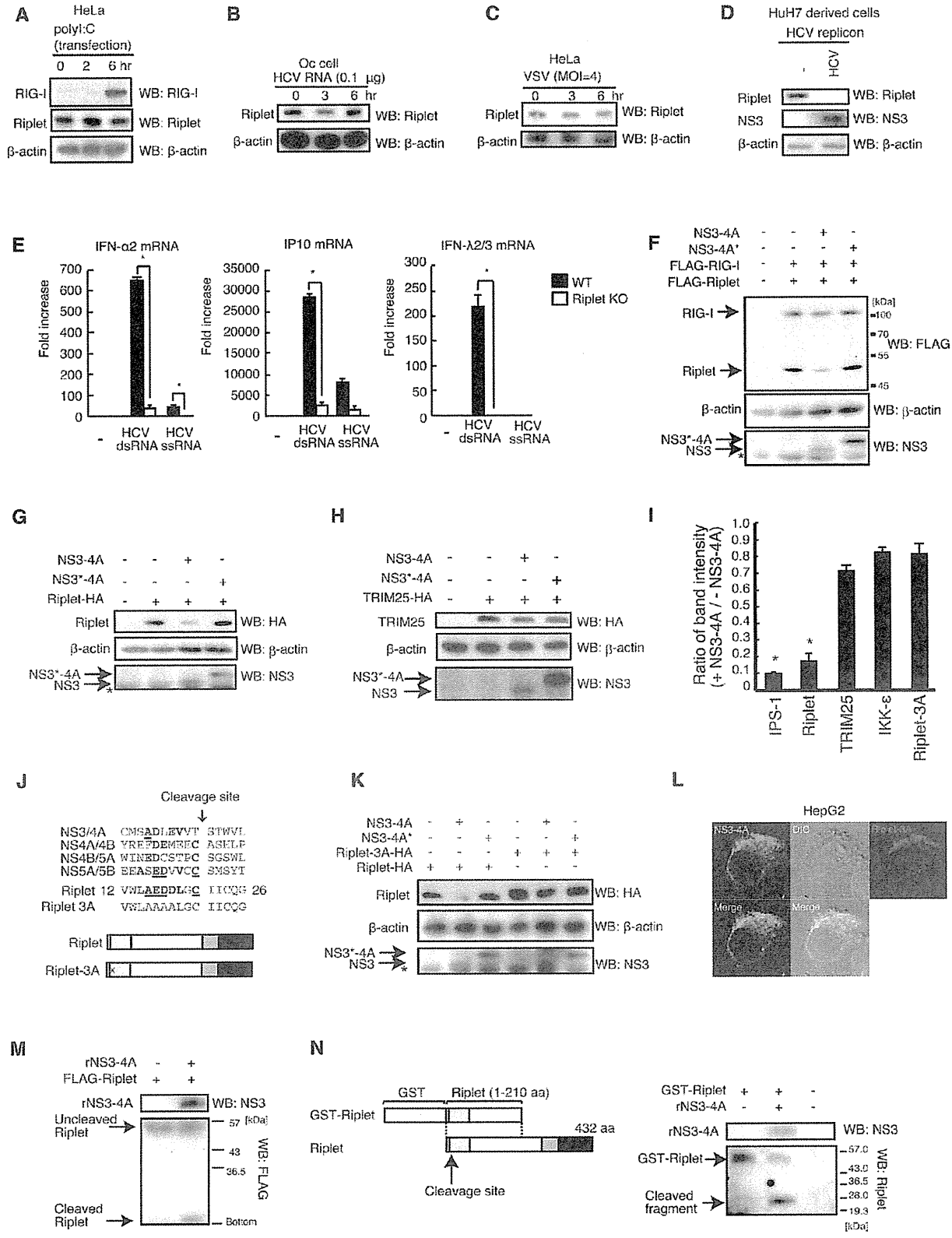
A
HeLa
poly I:C
(transfection)
0 2 6 hr
RIG-I
Riplet
β-actin
WB: RIG-I
WB: Riplet
WB: β-actin
B
Oc cell
HCV RNA (0.1 μg)
0 3 6 hr
Riplet
β-actin
WB: Riplet
WB: β-actin
C
HeLa
VSV (MOI=4)
0 3 6 hr
Riplet
β-actin
WB: Riplet
WB: β-actin
D
HuH7 derived cells
HCV replicon
-
HCV
Riplet
NS3
β-actin
WB: Riplet
WB: NS3
WB: β-actin
E
IFN-α2 mRNA
IP10 mRNA
IFN-λ2/3 mRNA
Fold increase
WT
Riplet KO
-
HCV dsRNA
HCV ssRNA
F
NS3-4A
NS3-4A*
FLAG-RIG-I
FLAG-Riplet
RIG-I
Riplet
β-actin
NS3*-4A
NS3
[kDa]
100
70
55
45
WB: FLAG
WB: β-actin
WB: NS3
G
NS3-4A
NS3*-4A
Riplet-HA
Riplet
β-actin
NS3*-4A
NS3
WB: HA
WB: β-actin
WB: NS3
H
NS3-4A
NS3*-4A
TRIM25-HA
TRIM25
β-actin
NS3*-4A
NS3
WB: HA
WB: β-actin
WB: NS3
I
Ratio of band intensity
(+ NS3-4A / - NS3-4A)
IPS-1
Riplet
TRIM25
IKK-ε
Riplet-3A
J
Cleavage site
NS3/4A CMSADLEVVT STWVL
NS4A/4B VREFDEMEEC ASHLP
NS4B/5A WINEDCSTPC SGSWL
NS5A/5B EEASEDVVCC SMSYT
Riplet 12 VWLAEDDLGC IICQG 26
Riplet 3A VWLAAAALGC IICQG
Riplet
Riplet-3A
K
NS3-4A
NS3-4A*
Riplet-3A-HA
Riplet-HA
Riplet
β-actin
NS3*-4A
NS3
WB: HA
WB: β-actin
WB: NS3
L
HepG2
NS3-4A
DIC
Riplet-3A
Merge
Merge
M
rNS3-4A
FLAG-Riplet
rNS3-4A
Uncleaved Riplet
Cleaved Riplet
WB: NS3
WB: FLAG
[kDa]
57
43
36.5
Bottom
N
GST
Riplet (1-210 aa)
GST-Riplet
Riplet
432 aa
Cleavage site
GST-Riplet
rNS3-4A
rNS3-4A
GST-Riplet
Cleaved fragment
WB: NS3
WB: Riplet
[kDa]

Figure 7. NS3-4A of HCV targets the Riplet protein. (A–D) Endogenous RIG-I and Riplet protein levels were observed by western blotting. HeLa cells were stimulated with polyI:C transfection (A), HCV dsRNA transfection (B) or infected with VSV (C). HCV replicon positive (HCV) and negative (-) cell lysates were prepared from a HuH7-derived cell line O cell that contains HCV 1b full-length replicons and O curred cell (Oc cell) in which HCV replicons were removed by IFN treatment (D). (E) The response to HCV RNA in wild-type and Riplet KO MEFs was examined by RT-qPCR. Wild type (WT) and Riplet knockout (KO) MEF cells were transfected with 100 ng of HCV ssRNA and dsRNA. Six hours after stimulation, mRNA expressions of IFN-α2, IP10, and IFN-λ2/3 were measured by RT-qPCR. Data are presented as mean ± SD (n = 3). *$p<0.05$. (F–H) FLAG-tagged Riplet and RIG-I (F), HA-tagged Riplet (G), or HA-tagged TRIM25 (H) expression vectors were transfected into HEK293FT cells together with NS3-4A or NS3-4A* expression vectors. NS3-4A* mutant protein harbors an amino acids substitution at its catalytic site Ser-139 with Ala. 24 hours after transfection, cell lysate was prepared and subjected to SDS-PAGE. (I) Band intensity ratio of IPS-1, Riplet, TRIM25, IKK-ε, and Riplet-3A with/without NS3-4A expression (mean ± sd, n = 3). (J) NS3-4A cleavage sites within an HCV polypeptide are compared with a candidate site in the Riplet RING-finger domain. Homologous amino acids are shown in bold, and identical amino acids are underlined. In Riplet-3A mutant protein, three acidic amino acids, Glu-16, Asp-17, Asp-18, were substituted with Ala. (K) An expression vector encoding wild-type Riplet or Ripled-3A mutant protein was transfected into HEK293 cells together with NS3-4A or NS3-4A* expression vectors. Cell lysate was prepared 24 hours after transfection, and subjected to SDS-PAGE. (L) HA-tagged Riplet-3A and NS3-4A expression vectors were transfected into HepG2 cell. 24 hours after transfection, the cells were fixed and stained with anti-HA monoclonal antibody (mouse) and anti-NS3-4A polyclonal antibody (goat). (M) N-terminal FLAG-tagged Riplet was expressed in HEK293FT cells, and immunoprecipitation was carried out with anti-FLAG antibody. Immunoprecipitates were incubated with recombination NS3-4A purified from *E.coli* at 37°C for one hour, and samples were subjected to SDS-PAGE analysis. The proteins were detected by western blotting. (N) Purified GST fused Riplet (1–210 aa) was incubated with or without recombinant NS3-4A (rNS3-4A) at 37°C for 30 min. The proteins were subjected to SDS-PAGE and detected by western blotting.

doi:10.1371/journal.ppat.1003533.g007

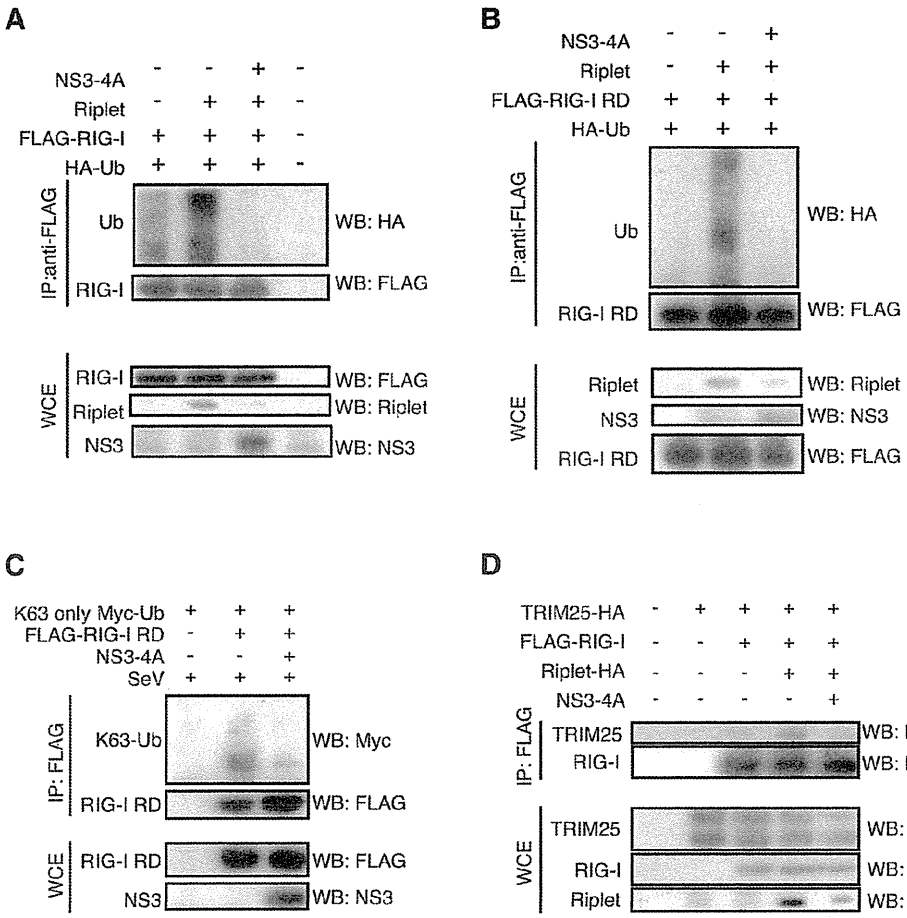

Figure 8. NS3-4A inhibits Riplet-mediated RIG-I polyubiquitination. (A, B) Riplet, NS3-4A, and/or HA-tagged ubiquitin (HA-Ub) expression vectors were transfected into HEK293FT cells along with either full-length RIG-I (A) or RIG-I RD (B). Cell lysate was prepared 24 hours after transfection, and subjected to SDS-PAGE. The proteins were detected by western blotting. (C). HEK293FT cells were transfected with Myc-tagged K63-only ubiquitin, FLAG-tagged RIG-I RD, and/or NS3-4A expression vectors. 24 hours after the transfection, cells were infected with SeV for six hours, and then cell lysate was prepared. Immunoprecipitation was carried out with anti-FLAG antibody, and the samples were subjected to SDS-PAGE. (D) HA-tagged TRIM25, Riplet and/or FLAG-tagged RIG-I expression vectors were transfected into HEK293FT cells with or without NS3-4A expression vector. Cell lysate was prepared 24 hours after the transfection, and immunoprecipitation assay was performed with anti-FLAG antibody. The precipitates were subjected to SDS-PAGE.

doi:10.1371/journal.ppat.1003533.g008

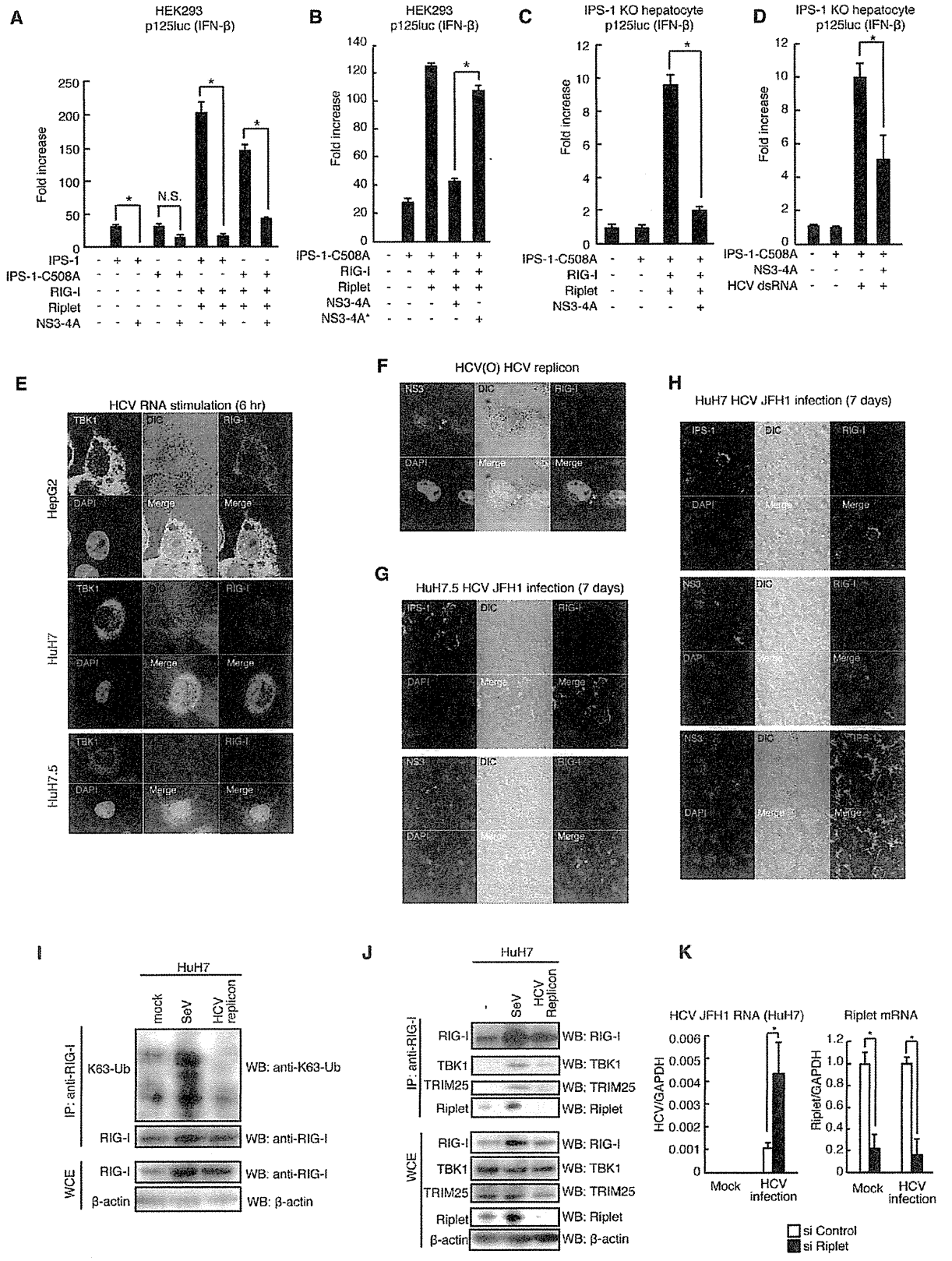
A
HEK293
p125luc (IFN-β)
Fold increase
IPS-1
IPS-1-C508A
RIG-I
Riplet
NS3-4A
N.S.
B
HEK293
p125luc (IFN-β)
Fold increase
IPS-1-C508A
RIG-I
Riplet
NS3-4A
NS3-4A*
C
IPS-1 KO hepatocyte
p125luc (IFN-β)
Fold increase
IPS-1-C508A
RIG-I
Riplet
NS3-4A
D
IPS-1 KO hepatocyte
p125luc (IFN-β)
Fold increase
IPS-1-C508A
NS3-4A
HCV dsRNA
E
HCV RNA stimulation (6 hr)
HepG2
HuH7
HuH7.5
TBK1
RIG-I
DAPI
Merge
F
HCV(O) HCV replicon
NS3
DIC
RIG-I
DAPI
Merge
G
HuH7.5 HCV JFH1 infection (7 days)
IPS-1
NS3
DIC
RIG-I
DAPI
Merge
H
HuH7 HCV JFH1 infection (7 days)
IPS-1
NS3
DIC
RIG-I
DAPI
Merge
I
HuH7
mock
SeV
HCV replicon
IP: anti-RIG-I
K63-Ub
RIG-I
WCE
RIG-I
β-actin
WB: anti-K63-Ub
WB: anti-RIG-I
WB: anti-RIG-I
WB: β-actin
J
HuH7
SeV
HCV Replicon
IP: anti-RIG-I
RIG-I
TBK1
TRIM25
Riplet
WCE
RIG-I
TBK1
TRIM25
Riplet
β-actin
WB: RIG-I
WB: TBK1
WB: TRIM25
WB: Riplet
WB: RIG-I
WB: TBK1
WB: TRIM25
WB: Riplet
WB: β-actin
K
HCV JFH1 RNA (HuH7)
HCV/GAPDH
Mock
HCV infection
Riplet mRNA
Riplet/GAPDH
Mock
HCV infection
si Control
si Riplet

Figure 9. HCV abrogated Riplet-mediated RIG-I activation. (A and B) The inhibition of IFN-β promoter activation by NS3-4A was assessed by reporter gene assays. IPS-1-C508A mutant protein harbors an amino acid substitution at Cys-508 with Ala. 100 ng of IPS-1, IPS-1-C508A, RIG-I, Riplet, NS3-4A, and/or NS3-4A* expression vectors were transfected into HEK293 cells in 24-well plates with p125luc reporter plasmid. The total amount of transfected DNA (800 ng/well) was kept constant by adding empty vector (pEF-BOS). 24 hours after the transfection, the reporter activities were measured. Data are presented as mean ± SD (n = 3). *$p<0.05$. (C and D) IPS-1 KO mouse hepatocyte was transfected with IPS-1 C508A, RIG-I, Riplet, and/or NS3-4A expression vectors together with p125luc and *Renilla* luciferase plasmids. Transfected cells were stimulated with 50 ng of HCV dsRNA for 24 hours by transfection (D). Data are presented as mean SD (n = 3). *$p<0.05$. (E and F) Intracellular localizations of endogenous TBK1 and RIG-I were determined by confocal microscopy. HepG2, HuH7, and HuH7.5 cells were stimulated with 100 ng of HCV dsRNA for six hours by transfection (E). Stimulated cells (E) and O cells with HCV replicons (F) were stained with anti-RIG-I, TBK1, and/or NS3 antibodies. (G and H) HuH7 (G) and HuH7.5 (H) cells were infected with HCV JFH1 strain. Seven days after the infection, the cells were stained with anti-RIG-I, IPS-1, and NS3 antibodies. (I) HuH7 cells were infected with SeV at MOI = 1 for 24 hours. Cell lysates were prepared from mock or SeV infected HuH7 or HuH7 cells with HCV replicons (O cell). Immunoprecipitation using high salt buffer was performed with anti-RIG-I (Alme-1) antibody. The samples were subjected to SDS-PAGE. Endogenous K63-linked polyubiquitin chain was detected using ubiquitin K63-linkage specific antibody. (J) HuH7 cells were infected with SeV at MOI = 1 for 24 hours. Cell lysates were prepared from mock or SeV infected HuH7 or HuH7 cells with HCV replicons (O cell). Immunoprecipitation was performed with anti-RIG-I (Alme-1) antibody. The samples were subjected to SDS-PAGE. (K) HuH7 cells were transfected with siRNA for mock or Riplet. 48 hours after the transfection, cells were infected with HCV JFH1 for 2 days. RT-qPCR was performed to determine HCV genome RNA, GAPDH, and Riplet expression.
doi:10.1371/journal.ppat.1003533.g009

inactive TBK1 and that TBK1 was activated after loading on to mitochondria (Figure 10).

HCV is a major cause of HCC and has the ability to evade host innate immune response [7,43]. HCV RNA is primarily recognized by the cytoplasmic viral RNA sensor RIG-I. Previous studies showed that the protease NS3-4A cleaves IPS-1 to shut off RIG-I signaling. However, our results indicated that there was another target of NS3-4A in RIG-I signaling. First, RIG-I failed to exhibit punctate staining in cells infected with HCV. Second, NS3-4A reduced RIG-I signaling even in the presence of an IPS-1-C508A mutant, which is resistant to the cleavage by NS3-4A. Third, the endogenous Riplet protein level was severely reduced in cells with HCV replicons. Fourth, NS3-4A targeted Riplet and abrogated Riplet-dependent RIG-I ubiquitination and complex formation with TRIM25 and TBK1. These data support our model that NS3-4A targets not only IPS-1 but also Riplet to escape host innate immune responses (Figure 10). Recently it was reported that NS1 proteins of Influenza A virus inhibited Riplet function [32]. These findings indicated biological importance of Riplet in RIG-I activation during viral infection.

In general, a ubiquitin ligase has several targets. We have performed yeast two-hybrid screening using Riplet as bait and found a candidate clone that encodes a tumor suppressor gene. Our pilot study showed that Riplet mediated K63-linked polyubiquitination of this tumor suppressor and suppressed retinoblastoma (Rb) activity. Thus, Riplet disruption by NS3-4A might be a cause of liver disease induced by HCV infection.

Materials and Methods

Ethics statement

All animal studies were carried out in strict accordance with Guidelines for Animal Experimentation of the Japanese Associations for Laboratory Animal Science. The protocols were approved by the Animal Care and Use Committee of Hokkaido University, Japan (Permit Number: 08-0245 and 09-0215).

Cell

HEK293, Vero, and HepG2 cells were cultured in Dulbecco's modified Eagle's medium low glucose medium (D-MEM) with 10% heat-inactivated fetal calf serum (FCS) (Invitrogen). HeLa cells were cultured in minimum Eagle's medium with 2 mM L-glutamine and 10% heat-inactivated FCS. HEK293FT cells were maintained in D-MEM high glucose medium containing 10% of heat-inactivated FCS (Invitrogen). Human hepatocyte cell line with HCV 1b full-length replicons (O cells) and O curred cells (Oc cells) were kindly gifted from Kato N [44]. O cells were cultured in D-MEM high glucose with 10% of heat-inactivated FCS, G418, NEAA, and L-Gln.

Viruses

VSV Indiana strain and SeV HVJ strain were amplified using Vero cells. To determine the virus titer, we performed plaque assay using Vero cells. HCV JFH1 was amplified using HuH7.5 cells.

Mice

Generation of IPS-1 KO and Riplet KO mice were described previously [23,45]. Splenocyte was isolated from C57BL/6 wild-type and Riplet KO mice. Isolated cells were cultured in RPMI1640 containing 10% of heat-inactivated FCS. The preparations of wild-type and Riplet KO MEFs were described previously [23]. Preparation of IPS-1 KO mouse hepatocyte was described previously [37]. All mice were maintained under specific-pathogen free conditions in the animal facility of the Hokkaido University Graduate School of Science (Japan).

Plasmids

Expression vectors encoding for N-terminal FLAG-tagged RIG-I, N-terminal FLAG-tagged RIG-I CARDs (dRIG-I), FLAG-tagged RIG-I ΔRD (RIG-I-dRD), FLAG-tagged RIG-I RD, C-terminal HA-tagged TRIM25, C-terminal HA-tagged Riplet, and Riplet-ΔRING (Riplet-DN) plasmids were described previously [21,23]. The amino acids substitutions from 16 to 18 with Ala was carried out by PCR-mediated mutagenesis using primers, Ripelt-3A-F and Riplet-3A-R and pEF-BOS/Riplet plasmid as a template. The primer sequence is Riplet-3A-F: TTC CCG TGT GGC TGG CCG CGG CCG CCC TCG GCT GCA TCA TCT GCC, and Riplet-3A-R: GGC AGA TGA TGC AGC CGA GGG CGG CCG CGG CCA GCC ACA CGG GAA. RIG-I K172R and RIG-I K788R expression vectors was constructed by PCR-mediated mutagenesis using primers, RIG-I K172R-F, RIG-I K172R-R, RIG-I K788R-F and RIG-I-K788R-R, and pEF-BOS/FLAG-RIG-I plasmid as a template. The primer sequences are RIG-I K172R-F: GGA AAA CTG GCC CAA AAC TTT GAG ACT TGC TTT GGA GAA AG, RIG-I K172R-R: CTT TCT CCA AAG CAA GTC TCA AAG TTT TGG GCC AGT TTT CC, RIG-I-K788R-F: TGC ATA TAC AGA CTC ATG AAA GAT TCA TCA GAG ATA GTC AAG AA, and RIG-I-K788-R: CTT GAC TAT CTC TGA TGA ATC TTT CAT GAG TCT GTA TAT GCA G. RIG-I 5KR expression vectors were constructed by PCR-mediated mutagenesis using primers, RIG-I 849 851 RR-F, RIG-I 849 851 RR-R, RIG-I 888R-F, RIG-I 888R-R, RIG-I 907 909 RR-F, RIG-I 907 909 RR-R, and

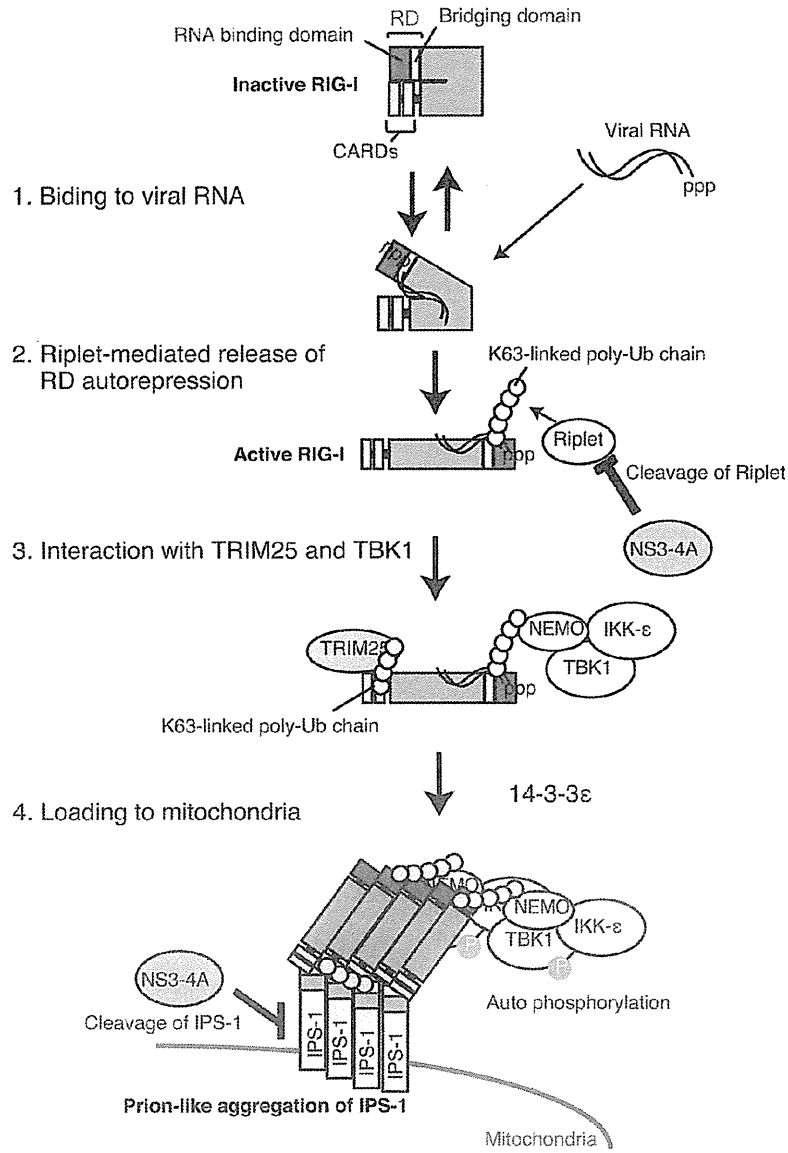

Figure 10. Model for Riplet-mediated RIG-I activation. In resting cell, RIG-I RD represses its CARDs-mediated signaling. When RIG-I CTD associates with viral RNA, Riplet mediates K63-linked polyubiquitination of RIG-I RD, leading to the association with TRIM25 and TBK1. K63-linked polyubiquitin chain mediated by TRIM25 induces RIG-I oligomerization and association with IPS-1 adaptor. TBK1 associated with RIG-I is activated on mitochondria.
doi:10.1371/journal.ppat.1003533.g010

pEF-BOS/FLAG-RIG-I plasmid as a template. The primer sequences are RIG-I 849 851 RR-F: AGT AGA CCA CAT CCC AGG CCA AGG CAG TTT TCA AGT TTT G, RIG-I 849 851 RR-R: CAA AAC TTG AAA ACT GCC TTG GCC TGG GAT GTG GTC TAC T, RIG-I 888R-F: GAC ATT TGA GAT TCC AGT TAT AAG AAT TGA AAG TTT TGT GGT GGA GG, RIG-I 888R: CCT CCA CCA CAA AAC TTT CAA TTC TTA TAA CTG GAA TCT CAA ATG TC, RIG-I 907 909RR-F: GTT CAG ACA CTG TAC TCG AGG TGG AGG GAC TTT CAT TTT GAG AAG, RIG-I 907 909RR-R: CTT CTC AAA ATG AAA GTC CCT CCA CCT CGA GTA CAG TGT CTG AAC. HCV cDNA fragment encoding NS3-4A of JFH1 strain was cloned into pCDNA3.1 (-) vector. The mutation on catalytic site of NS3-4A S139A was constructed by PCR-mediated mutagenesis using primers, NS3-4A S139A-F and NS3-4A S139A-R, and pCDNA3.1 (-)/NS3-4A plasmid as a template. The primer sequences are NS3-4A S139A-F: TTC GAC CTT GAA GGG GTC CGC GGG GGG ACC GGT GCT TTG C and NS3-4A S139A-R: AAG CAC CGG TCC CCC CGC GGA CCC CTT CAA GGT CGA AAG G.

RT-PCR and Real-Time PCR

Total RNA was extracted with TRIZOL (Invitrogen), after which the samples were treated with DNaseI to remove DNA

contamination. Reverse transcription was performed using High Capacity cDNA Reverse Transcription Kit (ABI). Quantitative PCR analysis was performed using Step One software ve2.0. (ABI) with SYBER Green Master Mix (ABI). HCV ss and dsRNA was in vitro synthesized with SP6 and/or T7 RNA polymerase using 3′ UTR of HCV cDNA as template as described previously [46].

Confocal microscopy

Cells were plated onto microscope cover glasses (matsunami) in a 24-well plate. The cells were fixed for 30 min using 3% formaldehyde in PBS and permeabilized with 0.2% Triton X-100 for 15 min. Fixed cells were blocked with 1% bovine serum albumin in PBS for 10 min and labeled with the indicated primary Abs for 60 min at room temperature. Alexa-conjugated secondary Abs were incubated for 30 min at room temperature to visualize staining of the primary Ab staining. Samples were mounted on glass slides using Prolong Gold (Invitrogen). Cells were visualized at a magnification of ×63 with an LSM510 META microscope (Zeiss). Data collected with confocal microscopy were analyzed with ZEISS LSM Image Examiner software. NS3, RIG-I, TBK1, IPS-1, and p-TBK1 were stained with anti-NS3 goat pAb (abcam), anti-RIG-I mouse mAb (Alme-1, ALEXIS BIOCHEMICALS), anti-NAK (TBK1) rabbit mAb (EP611Y, abcam), anti-MAVS (IPS-1) rabbit pAb (Bethyl Laboratories Inc), and anti-p-TBK1 rabbit mAb (Cell Signaling Technology),

Reporter gene analysis

HEK293 cells were transiently transfected in 24-well plates using FuGene HD (Promega) or lipofectamine 2000 (Invitrogen) with expression vectors, reporter plasmids (IFN-β: p125luc), and an internal control plasmid coding *Renilla* luciferase. The total amounts of plasmids were normalized using an empty vector. Cells were lysed in a lysis buffer (Promega), and luciferase and *Renilla* luciferase activities were determined using a dual luciferase assay kit (Promega). Relative luciferase activities were calculated by normalizing the luciferase activity by control. HCV dsRNA (3′ UTR polyU/UC region) was synthesized using T7 and SP6 RNA polymerase as described previously [46].

Pull-down assay

RNA used for the assay was purchased from JBioS. The RNA sequences are as follows: (sense strand) AAA CUG AAA GGG AGA AGU GAA AGU G; and (antisense strand) CAC UUU CAC UUC UCC CUU UCA GUU U. Biotin was conjugated at the U residue at the 3′-end of the antisense strand (underlined). Biotinylated dsRNA was phosphorylated by T4 polynucleotide kinase (TAKARA). dsRNA was incubated for one hour at 25°C with 10 μg of protein from the cytoplasmic fraction of cells that were transfected with Flag-tagged RIG-I, Riplet, and/or HA-tagged ubiquitin expressing vectors. This mixture was added into 400 μl of lysis buffer (20 mM Tris-HCl pH 7.5, 150 mM NaCl, 1 mM EDTA, 10% Glycerol, 1% NP-40, 30 mM NaF, 5 mM Na_3VO_4, 20 mM iodoacetamide, and 2 mM PMSF) containing 25 μl of streptavidine Sepharose beads, rocked at 4°C for two hours, harvested by centrifugation, washed three times with lysis buffer, and resuspended in SDS sample buffer.

Immunoprecipitation

Splenocytes (1×10^7) were infected with or without VSV at MOI = 10 for eight hours, after which cell extracts were prepared with lysis buffer (20 mM Tris-HCl pH 7.5, 150 mM NaCl, 1 mM EDTA, 10% glycerol, 1% Nonidet P-40, 30 mM NaF, 5 mM Na_3VO_4, 20 mM iodoacetamide, and 2 mM phenylmethylsulfonyl fluoride). Immunoprecipitation used an anti-RIG-I Rabbit monoclonal antibody (D14G6, Cell Signaling Technology). To detect endogenous K63-linked polyubiquitin chain that is ligated to RIG-I, 6×10^7 of mouse splenocyte were infected with SeV at MOI = 0.2 for 24 hours. Immunoprecipitation was performed with anti-RIG-I mAb (D14G6). Anti-K63-linkage specific polyubiquitin (D7A11) Rabbit mAb (Cell Signaling) was used for western blotting. HEK293FT cells were transfected with or without 0.8 μg of HCV dsRNA in a 6-well plate. HCV dsRNA (HCV 3′ UTR polyU/UC region) was synthesized using T7 and SP6 RNA polymerase as previously described [46]. Cell lysates were prepared at the indicated times. Immunoprecipitation was performed with an anti-RIG-I mouse monoclonal antibody (Alme-1). An anti-FLAG M2 monoclonal antibody (Sigma) was used for the immunoprecipitation of FLAG-tagged protein. An anti-TRIM25 rabbit polyclonal antibody (abcam), an anti-p-TBK1 rabbit mAb (Cell Signaling Technology), an anti-NAK (TBK1) rabbit mAb (EP611Y), and an anti-RNF135 (Riplet) pAb (SIGMA), were used for western blotting. For ubiquitination assay, immunoprecipitates were washed three times with high salt lysis buffer ((20 mM Tris-HCl pH 7.5, 1M NaCl, 1 mM EDTA, 10% glycerol, 1% Nonidet P-40, 30 mM NaF, 5 mM Na_3VO_4, 20 mM iodoacetamide, and 2 mM phenylmethylsulfonyl fluoride) to dissociate unanchored polyubiquitin chain [21], and then washed once with normal lysis buffer described above for SDS-PAG analysis. Band intensity was semi-quantified using Photoshop software.

RNAi

siRNAs for human Riplet (Silencer Select Validated siRNA) and negative control were purchased from Ambion. siRNA sequences for Riplet are: (sense) GGA ACA UCU UGU AGA CAU Utt and (anti-sense) AAU GUC UAC AAG AUG UUC CCac. siRNA was transfected into cells using RNAiMax Reagent (Invitrogen) according to the manufacture's instructions.

In vitro NS3/4A cleavage assay

FLAG-tagged Riplet was expressed in HEK293FT cells, and cell lysate was prepared with the lysis buffer described above. The protein was immunoprecipitated with anti-FLAG antibody and protein G sepharose beads, and washed with Buffer B (20 mM Tris-HCl pH 7.5, 150 mM NaCl, 10% glycerol, 1% Nonidet P-40). The samples were suspended in 50 μl of Buffer B, and incubated with 400 ng of recombinant NS3-4A (rNS3-4A) protein at 37°C for one hour, and then subjected to SDS-PAGE analysis. The NS3-4A protein was purchased from AnaSpec Inc (CA). N-terminal GST-fused Riplet (1–210 aa) (rRiplet) was purchased from Abnova. 500 ng of rRiplet was incubated with or without 500 ng of rNS3-4A in 10 μl of reaction buffer (20 mM Tris-HCl (7.5), 4% Glycerol, 5 mM DTT, 150 mM NaCl, 0.1% of Triton-X100, 0.9% polyvinyl alcohol) at 37°C for 30 min.

Accession numbers

The accession numbers are Riplet (BAG84604), TRIM25 (NP_005073), TBK1 (NP_037386), IKK-ε (AAF45307), IPS-1 (BAE79738), RIG-I (NP_055129), and G3BP (CAG38772).

Supporting Information

Figure S1 K63-linked polyubiquitination of RIG-I RD. HA-tagged ubiquitin and FLAG-tagged RIG-I RD expression vectors were transfected into HEK293FT cells. 24 hours after transfection, the cells were infected with VSV at MOI = 1 for six

hours. Then, cell lysate was prepared. Immunoprecipitation was carried out using anti-FLAG antibody. The samples were subjected to SDS-PAGE, and the proteins were detected by western blotting using anti-HA, FLAG, and K63-linked poly-ubiquitin specific antibodies.
(TIF)

Figure S2 Intracellular localization of RIG-I, NEMO, and p-TBK1 proteins. (A) HeLa cells were transfected with HCV dsRNA using lipofectamine 2000 reagent. The cells were fixed six hours after transfection. The microscopic analysis was performed using anti-RIG-I mAb (Alme-1) and anti-NEMO pAb. (B) HeLa cells were transfected with HCV dsRNA using lipofectamine 2000 reagent (Invitrogen). The cells were fixed at indicated hour. The microscopic analysis was performed using anti-RIG-I mAb (Alme-1). (C) HepG2 cells were transfected with HCV dsRNA using lipofectamine 200 reagent. The cells were fixed six hours after the transfection. The microscopic analysis was performed using anti-RIG-I (Alme-1) mAb and anti-p-TBK1 mAb.
(TIF)

Figure S3 NS3-4A of HCV cleaves IPS-1 and Riplet but not IKK-ε. (A) HA-tagged Riplet was transfected into HEK293 cells together with NS3-4A. 24 hours after transfection, cell lysate was prepared and subjected to SDS-PAGE. The proteins were detected by western blotting and CBB staining. (B, C) HA-tagged IKK-ε (B) or IPS-1 (C) expression vectors were transfected into HEK293FT cells with or without NS3-4A of HCV expression vector. 24 hours after the transfection, the cell lysate was prepared, and analyzed by SDS-PAGE. The proteins were detected by western blotting using anti-HA or anti-β actin antibodies. (D) HA-tagged IPS-1 or HA-tagged Riplet expression vector was transfected into HEK293FT cells with or without NS3-4A expression vectors. 24 hours after transfection, cell lysate was prepared and subjected to SDS-PAGE. The proteins were detected by western blotting using anti-HA antibody. (E, F) N-terminal FLAG-tagged Riplet (E) or C-terminal HA-tagged Riplet (F) expression vector was transfected into HEK293FT cells with NS3-4A or NS3-4A*. 24 hours after the transfection, cell lysates were analyzed by SDS-PAGE. (G) HA-tagged wild-type Riplet or mutant Riplet-C21A expression vector were transfected into HEK293FT cells with NS3-4A or NS3-4A*. 24 hours after the transfection, the cell lysate was prepared, and analyzed by SDS-PAGE. The proteins were detected by western blotting using anti-HA or anti-β actin antibodies. (H, I) RIG-I, Riplet, Riplet-3A (H), and/or Riplet C21A (I) mutant expression vectors were transfected into HEK293 cells together with p125luc reporter and *Renilla* luciferase. 24 hours after transfection, luciferase activity was measured.
(TIF)

Figure S4 siRNA for Riplet or control was transfected into HeLa cells in 24-well plate using RNAi MAX (Invitrogen) according to manufacture's protocol. 48 hours after transfection, the cells were transfected with 100 ng of HCV dsRNA. Six hours after transfection, the cells were fixed and stained with anti-RIG-I mAb (Alme-1) and anti-mouse Alexa-488 Ab.
(TIF)

Acknowledgments

We thank Dr. Shimotohno K (Chiba institute of Technology), Dr. Fujita T (Kyoto University), and Dr. Sasai M (Osaka University) for critical comments, and Suzuki T for help on microscopic analysis. O and Oc cells were kindly gifted from Kato N [44].

Author Contributions

Conceived and designed the experiments: HO MMi MMa TS. Performed the experiments: HO MMi. Analyzed the data: HO MMi. Contributed reagents/materials/analysis tools: HO MMi. Wrote the paper: HO MMi TS.

References

1. Kato H, Takeuchi O, Sato S, Yoneyama M, Yamamoto M, et al. (2006) Differential roles of MDA5 and RIG-I helicases in the recognition of RNA viruses. Nature 441: 101–105.
2. Yoneyama M, Kikuchi M, Natsukawa T, Shinobu N, Imaizumi T, et al. (2004) The RNA helicase RIG-I has an essential function in double-stranded RNA-induced innate antiviral responses. Nat Immunol 5: 730–737.
3. Saito T, Hirai R, Loo YM, Owen D, Johnson CL, et al. (2007) Regulation of innate antiviral defenses through a shared repressor domain in RIG-I and LGP2. Proc Natl Acad Sci U S A 104: 582–587.
4. Kowalinski E, Lunardi T, McCarthy AA, Louber J, Brunel J, et al. (2011) Structural basis for the activation of innate immune pattern-recognition receptor RIG-I by viral RNA. Cell 147: 423–435.
5. Xu LG, Wang YY, Han KJ, Li LY, Zhai Z, et al. (2005) VISA is an adapter protein required for virus-triggered IFN-beta signaling. Mol Cell 19: 727–740.
6. Seth RB, Sun L, Ea CK, Chen ZJ (2005) Identification and characterization of MAVS, a mitochondrial antiviral signaling protein that activates NF-kappaB and IRF 3. Cell 122: 669–682.
7. Meylan E, Curran J, Hofmann K, Moradpour D, Binder M, et al. (2005) Cardif is an adaptor protein in the RIG-I antiviral pathway and is targeted by hepatitis C virus. Nature 437: 1167–1172.
8. Kawai T, Takahashi K, Sato S, Coban C, Kumar H, et al. (2005) IPS-1, an adaptor triggering RIG-I- and Mda5-mediated type I interferon induction. Nat Immunol 6: 981–988.
9. Zhao T, Yang L, Sun Q, Arguello M, Ballard DW, et al. (2007) The NEMO adaptor bridges the nuclear factor-kappaB and interferon regulatory factor signaling pathways. Nat Immunol 8: 592–600.
10. McWhirter SM, Fitzgerald KA, Rosains J, Rowe DC, Golenbock DT, et al. (2004) IFN-regulatory factor 3-dependent gene expression is defective in Tbk1-deficient mouse embryonic fibroblasts. Proc Natl Acad Sci U S A 101: 233–238.
11. Hemmi H, Takeuchi O, Sato S, Yamamoto M, Kaisho T, et al. (2004) The roles of two IkappaB kinase-related kinases in lipopolysaccharide and double stranded RNA signaling and viral infection. J Exp Med 199: 1641–1650.
12. Lo YC, Lin SC, Rospigliosi CC, Conze DB, Wu CJ, et al. (2009) Structural basis for recognition of diubiquitins by NEMO. Mol Cell 33: 602–615.
13. Fitzgerald KA, McWhirter SM, Faia KL, Rowe DC, Latz E, et al. (2003) IKKepsilon and TBK1 are essential components of the IRF3 signaling pathway. Nat Immunol 4: 491–496.
14. Oshiumi H, Matsumoto M, Seya T (2012) Ubiquitin-mediated modulation of the cytoplasmic viral RNA sensor RIG-I. J Biochem 151: 5–11.
15. Gack MU, Shin YC, Joo CH, Urano T, Liang C, et al. (2007) TRIM25 RING-finger E3 ubiquitin ligase is essential for RIG-I-mediated antiviral activity. Nature 446: 916–920.
16. Liu HM, Loo YM, Horner SM, Zornetzer GA, Katze MG, et al. (2012) The Mitochondrial Targeting Chaperone 14-3-3epsilon Regulates a RIG-I Translocon that Mediates Membrane Association and Innate Antiviral Immunity. Cell Host Microbe 11: 528–537.
17. Arnaud N, Dabo S, Akazawa D, Fukasawa M, Shinkai-Ouchi F, et al. (2011) Hepatitis C virus reveals a novel early control in acute immune response. PLoS Pathog 7: e1002289.
18. Jiang X, Kinch LN, Brautigam CA, Chen X, Du F, et al. (2012) Ubiquitin-Induced Oligomerization of the RNA Sensors RIG-I and MDA5 Activates Antiviral Innate Immune Response. Immunity 36: 959–973.
19. Zeng W, Sun L, Jiang X, Chen X, Hou F, et al. (2010) Reconstitution of the RIG-I pathway reveals a signaling role of unanchored polyubiquitin chains in innate immunity. Cell 141: 315–330.
20. Friedman CS, O'Donnell MA, Legarda-Addison D, Ng A, Cardenas WB, et al. (2008) The tumour suppressor CYLD is a negative regulator of RIG-I-mediated antiviral response. EMBO Rep 9: 930–936.
21. Oshiumi H, Matsumoto M, Hatakeyama S, Seya T (2009) Riplet/RNF135, a RING finger protein, ubiquitinates RIG-I to promote interferon-beta induction during the early phase of viral infection. J Biol Chem 284: 807–817.
22. Gao D, Yang YK, Wang RP, Zhou X, Diao FC, et al. (2009) REUL is a novel E3 ubiquitin ligase and stimulator of retinoic-acid-inducible gene-I. PLoS One 4: e5760.
23. Oshiumi H, Miyashita M, Inoue N, Okabe M, Matsumoto M, et al. (2010) The ubiquitin ligase Riplet is essential for RIG-I-dependent innate immune responses to RNA virus infection. Cell Host Microbe 8: 496–509.
24. Saito T, Owen DM, Jiang F, Marcotrigiano J, Gale M, Jr. (2008) Innate immunity induced by composition-dependent RIG-I recognition of hepatitis C virus RNA. Nature 454: 523–527.

25. Foy E, Li K, Wang C, Sumpter R, Jr., Ikeda M, et al. (2003) Regulation of interferon regulatory factor-3 by the hepatitis C virus serine protease. Science 300: 1145–1148.
26. Li XD, Sun L, Seth RB, Pineda G, Chen ZJ (2005) Hepatitis C virus protease NS3/4A cleaves mitochondrial antiviral signaling protein off the mitochondria to evade innate immunity. Proc Natl Acad Sci U S A 102: 17717–17722.
27. Ebihara T, Shingai M, Matsumoto M, Wakita T, Seya T (2008) Hepatitis C virus-infected hepatocytes extrinsically modulate dendritic cell maturation to activate T cells and natural killer cells. Hepatology 48: 48–58.
28. Li K, Foy E, Ferreon JC, Nakamura M, Ferreon AC, et al. (2005) Immune evasion by hepatitis C virus NS3/4A protease-mediated cleavage of the Toll-like receptor 3 adaptor protein TRIF. Proc Natl Acad Sci U S A 102: 2992–2997.
29. Arimoto K, Takahashi H, Hishiki T, Konishi H, Fujita T, et al. (2007) Negative regulation of the RIG-I signaling by the ubiquitin ligase RNF125. Proc Natl Acad Sci U S A 104: 7500–7505.
30. Onomoto K, Jogi M, Yoo JS, Narita R, Morimoto S, et al. (2012) Critical role of an antiviral stress granule containing RIG-I and PKR in viral detection and innate immunity. PLoS One 7: e43031.
31. Kageyama M, Takahasi K, Narita R, Hirai R, Yoneyama M, et al. (2011) 55 Amino acid linker between helicase and carboxyl terminal domains of RIG-I functions as a critical repression domain and determines inter-domain conformation. Biochem Biophys Res Commun 415: 75–81.
32. Rajsbaum R, Albrecht RA, Wang MK, Maharaj NP, Versteeg GA, et al. (2012) Species-Specific Inhibition of RIG-I Ubiquitination and IFN Induction by the Influenza A Virus NS1 Protein. PLoS Pathog 8: e1003059.
33. Soulat D, Burckstummer T, Westermayer S, Goncalves A, Bauch A, et al. (2008) The DEAD-box helicase DDX3X is a critical component of the TANK-binding kinase 1-dependent innate immune response. EMBO J 27: 2135–2146.
34. Gack MU, Albrecht RA, Urano T, Inn KS, Huang IC, et al. (2009) Influenza A virus NS1 targets the ubiquitin ligase TRIM25 to evade recognition by the host viral RNA sensor RIG-I. Cell Host Microbe 5: 439–449.
35. Bartenschlager R, Ahlborn-Laake L, Yasargil K, Mous J, Jacobsen H (1995) Substrate determinants for cleavage in cis and in trans by the hepatitis C virus NS3 proteinase. J Virol 69: 198–205.
36. Borden KL, Freemont PS (1996) The RING finger domain: a recent example of a sequence-structure family. Curr Opin Struct Biol 6: 395–401.
37. Aly HH, Oshiumi H, Shime H, Matsumoto M, Wakita T, et al. (2011) Development of mouse hepatocyte lines permissive for hepatitis C virus (HCV). PLoS One 6: e21284.
38. Gack MU, Kirchhofer A, Shin YC, Inn KS, Liang C, et al. (2008) Roles of RIG-I N-terminal tandem CARD and splice variant in TRIM25-mediated antiviral signal transduction. Proc Natl Acad Sci U S A 105: 16743–16748.
39. Takahasi K, Yoneyama M, Nishihori T, Hirai R, Kumeta H, et al. (2008) Nonself RNA-sensing mechanism of RIG-I helicase and activation of antiviral immune responses. Mol Cell 29: 428–440.
40. Paz S, Vilasco M, Arguello M, Sun Q, Lacoste J, et al. (2009) Ubiquitin-regulated recruitment of IkappaB kinase epsilon to the MAVS interferon signaling adapter. Mol Cell Biol 29: 3401–3412.
41. Zeng W, Xu M, Liu S, Sun L, Chen ZJ (2009) Key role of Ubc5 and lysine-63 polyubiquitination in viral activation of IRF3. Mol Cell 36: 315–325.
42. Oganesyan G, Saha SK, Guo B, He JQ, Shahangian A, et al. (2006) Critical role of TRAF3 in the Toll-like receptor-dependent and -independent antiviral response. Nature 439: 208–211.
43. Suzuki T, Ishii K, Aizaki H, Wakita T (2007) Hepatitis C viral life cycle. Adv Drug Deliv Rev 59: 1200–1212.
44. Ikeda M, Abe K, Dansako H, Nakamura T, Naka K, et al. (2005) Efficient replication of a full-length hepatitis C virus genome, strain O, in cell culture, and development of a luciferase reporter system. Biochem Biophys Res Commun 329: 1350–1359.
45. Oshiumi H, Okamoto M, Fujii K, Kawanishi T, Matsumoto M, et al. (2011) The TLR3/TICAM-1 pathway is mandatory for innate immune responses to poliovirus infection. J Immunol 187: 5320–5327.
46. Oshiumi H, Ikeda M, Matsumoto M, Watanabe A, Takeuchi O, et al. (2010) Hepatitis C virus core protein abrogates the DDX3 function that enhances IPS-1-mediated IFN-beta induction. PLoS One 5: e14258.

JVI
Journals.ASM.org

Herpesvirus 6 Glycoproteins B (gB), gH, gL, and gQ Are Necessary and Sufficient for Cell-to-Cell Fusion

Yuki Tanaka,[a] Tadahiro Suenaga,[a,b] Misako Matsumoto,[c] Tsukasa Seya,[c] Hisashi Arase[a,b,d]

Department of Immunochemistry, Research Institute for Microbial Diseases, Osaka University, Osaka, Japan[a]; Laboratory of Immunochemistry, WPI Immunology Frontier Research Center, Osaka University, Osaka, Japan[b]; Department of Microbiology and Immunology, Graduate School of Medicine, Hokkaido University, Sapporo, Japan[c]; CREST, JST, Tokyo, Japan[d]

The human herpesvirus 6 (HHV-6) envelope glycoprotein gH/gL/gQ1/gQ2 complex associates with host cell CD46 as its cellular receptor. Although gB has been suggested to be involved in HHV-6 infection, its function in membrane fusion has remained unclear. Here, we have developed an HHV-6A (strain GS)and HHV-6B (strain Z29) virus-free cell-to-cell fusion assay and demonstrate that gB and the gH/gL/gQ1/gQ2 complex are the minimum components required for membrane fusion by HHV-6.

Human herpesvirus 6 (HHV-6), betaherpesvirus subfamily (1), includes two species, A (HHV-6A) and B (HHV-6B) (2–4). HHV-6B mainly infects immune cells, such as $CD4^+$ T-lymphocytes, monocytes, and dendritic cells, and also causes exanthema subitum during primary infection in children (5). HHV-6B can reactivate from latency in immunocompromised patients and cause pneumonitis, hepatitis, and encephalitis (6, 7). However, the molecular basis of HHV-6A pathogenicity is unclear.

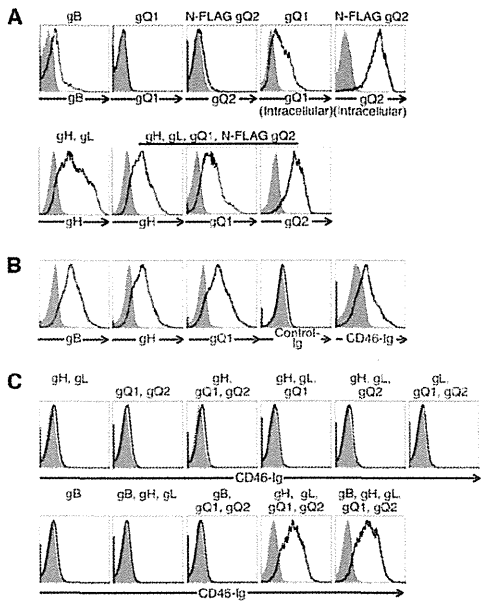

FIG 1 Flow cytometric analyses of cell surface expression of viral glycoproteins in cells transfected with plasmids expressing the glycoproteins. The transfected glycoprotein(s) is shown at the top of each figure panel. gQ2 was FLAG tagged. (A) Expression of HHV-6B glycoprotein(s) in 293T cells transfected with plasmids expressing HHV-6B glycoprotein(s) (black lines) or mock transfected (gray-shaded areas). Cells were stained with anti-gB (H-AR-2; Bioworld Consulting Laboratories), anti-gH, anti-gQ1 (2D6; NIH, AIDS Reagent Program), or FLAG (L5; Biolegend) MAb followed by staining with anti-mouse IgG antibody. (B) Cell surface expresson of HHV-6B glycoproteins in virus-infected cells and association of CD46 with HHV-6B-infected cells. HHV-6B-infected (black lines) or mock-infected (gray-shaded areas) Molt-3 cells were stained with anti-gB, anti-gH, or anti-gQ1 MAb followed by staining with anti-mouse IgG antibody and either CD46-Ig or control Ig (VZV gB-Ig) followed by staining with anti-human IgG Fc portion antibody. (C) Association of CD46 with HHV-6B glycoproteins. 293T cells that were transfected with plasmids expressing HHV-6B glycoprotein(s) (black lines) or mock transfected (gray-shaded areas) were stained with CD46-Ig.

The association of several viral glycoproteins with their respective cellular receptors induces virus envelope-cell membrane fusion during viral entry. It has been reported that HHV-6 gH/gL forms a complex with gQ1 and gQ2 and that this complex binds to CD46, which has been reported to function as a cellular receptor for HHV-6 (8–11). gB and a gH/gL complex are conserved in all herpesviruses and thought to play a pivotal role in membrane fusion and herpesvirus infection (12–17). Studies of gBs and gHs of other herpesviruses have elucidated the molecular mechanisms of virus envelope-cell membrane fusion (18–21). Although some antibodies against HHV-6 gB have been reported to block HHV-6B infection (22, 23), the function of HHV-6 gB during viral infection remains unclear.

To identify the requirement of HHV-6 glycoproteins for virus-induced membrane fusion during the virus infection, each of the glycoproteins was amplified and expressed from HHV-6B (Z29). Briefly, the genomic sequences of gH, gL, gO, gQ1, and gQ2 were amplified from total DNA of HHV-6B-infected Molt3 cells (Riken BRC, Tsukuba, Japan) and cloned into pCAGGS-MCS expression vector (24). For detection purposes, the FLAG epitope was inserted in frame at the N termini of gO and gQ2 genes. The full-length gB gene containing a promoter and poly(A) tail sequences was amplified by recombinant PCR using plasmids containing partial gB sequences (nucleotides [nt] +1 to +1718 and +1713 to +2493). The purified PCR product was used for transient transfection of 293T cells. Expression of transfected genes was analyzed by flow cytometry. gB and the gH/gL complex were detected on the cell surface using anti-gB monoclonal antibody (MAb) and gHA2 antibody, respectively (Fig. 1A) (25). Cells transfected with plasmid encoding gQ1 or N-terminal FLAG-tagged gQ2 ex-

Received 4 June 2013 Accepted 16 July 2013
Published ahead of print 24 July 2013
Address correspondence to Tadahiro Suenaga, tsue@biken.osaka-u.ac.jp.

doi:10.1128/JVI.01427-13

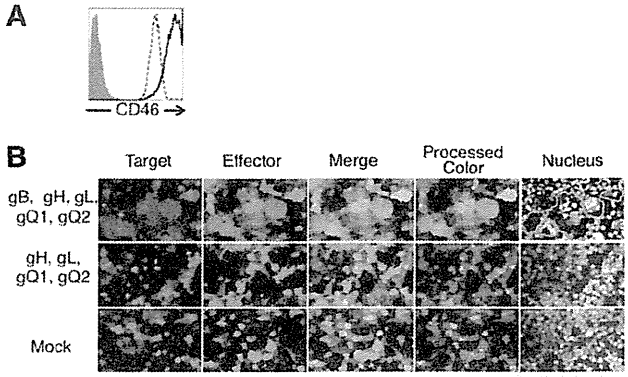

FIG 2 Fluorescence microscopy of fusion of 293T effector and target cells. (A) To quantify CD46 expression on the surface of 293T cells, 293T cells were stained with anti-CD46 MAb (J4.48; Coulter) (dotted line) or with isotype control antibody (gray-shaded area), and CD46-transfected 293T cells were stained with anti-CD46 MAb (solid line) and analyzed by flow cytometry. (B) 293T effector cells were transfected with plasmids expressing HHV-6B glycoproteins or mock transfected with a plasmid expressing DsRed. 293T target cells were transfected with a plasmid expressing CD46 and a plasmid expressing GFP. After 72 h coculture, cells were analyzed by fluorescence microscopy. Cell nuclei were stained with Hoechst 33258 fluorescence dye; blue fluorescence from nuclei appears gray. Fused cells are delineated by red lines.

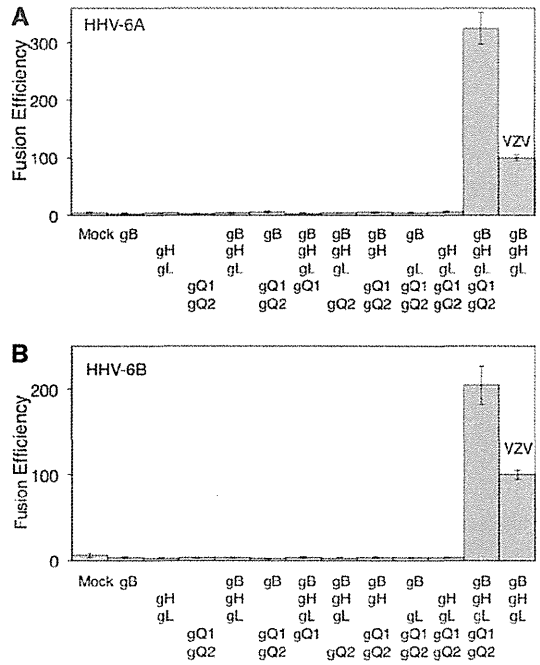

FIG 3 Quantification of cell-to-cell fusion mediated by HHV-6 glycoproteins. (A) 293T effector cells transfected with plasmids expressing HHV-6A glycoproteins, T7 polymerase, and *Renilla* luciferase were cocultured with 293T target cells transfected with plasmids expressing CD46 and firefly luciferase. After 72 h coculture, both luciferase signals were measured. The relative fusion efficiency was calculated as follows: [(HHV-6 firefly luciferase activity/HHV-6 *Renilla* luciferase activity) × 100]/(VZV firefly luciferase activity/VZV *Renilla* luciferase activity). (B) Quantification of cell-to-cell fusion efficiency mediated by HHV-6B glycoproteins was performed as described for HHV-6A in the panel A legend. Error bars show the means ± standard deviations (SD) of the results determined with quadruplicated samples. Data are representative of at least three independent experiments.

pressed the corresponding proteins. gQ1 and gQ2 were detected intracellularly but not on the cell surface, although they were detected on the surface of cells cotransfected with gH and gL. N-terminal FLAG-tagged gO was also expressed only on the surface of cells cotransfected with gH and gL (data not shown). The level of gB expression on HHV-6B-infected cells was higher than on gB-transfected cells. However, the levels of gH and gQ1 expression on transfected cells were higher than on infected cells (Fig. 1A and B).

We then generated a flow cytometry analysis that used CD46-Ig fusion protein to analyze HHV-6B glycoproteins that bind to CD46 (26). CD46-Ig specifically associated with HHV-6B-infected Molt-3 cells but not mock-infected cells (Fig. 1B). The 293T cells which were transfected with HHV-6 glycoprotein(s) and stained with CD46-Ig showed that CD46-Ig did not bind to cells expressing gH and gL, gB alone, or gH, gL, and gB but did bind to cells transfected with gH, gL, gQ1, and gQ2 (Fig. 1C). Expression of gB did not affect CD46-Ig binding to cells expressing gH, gL, gQ1, and gQ2. These results suggested that CD46 associated with a gH/gL/gQ1/gQ2 complex on the cell surface.

To identify HHV-6 glycoproteins that mediate membrane fusion, we developed a HHV-6 virus-free cell-to-cell fusion assay. 293T effector cells were cotransfected with the plasmids expressing HHV-6B glycoproteins and a plasmid expressing DsRed or were mock transfected. 293T target cells were cotransfected with plasmid expressing CD46 and green fluorescent protein (GFP) (Fig. 2A). Effector cells were cocultured with target cells 24 h after transfection. After coculture for 72 h, the cells were analyzed by fluorescence microscopy. As shown in Fig. 2B, yellow, giant, fused cells were observed when effector cells were cotransfected with plasmids expressing HHV-6B gB, gH, gL, gQ1, and gQ2 and cocultured with CD46-transfected target cells. However, no fused cells were found in the absence of gB.

To quantify fusion efficiency, a dual-luciferase reporter assay was used as previously reported (15). 293T effector cells were cotransfected with plasmid expressing HHV-6B glycoproteins, T7 polymerase (pCAGT7), and *Renilla* luciferase (as an internal control) and cocultured with 293T target cells transfected with CD46 and T7 promoter-driven firefly luciferase (pT7EMCluc) for 72 h. Firefly and *Renilla* luciferase activities were then measured, and fusion efficiency was calculated as described in the Fig. 3 legend. The fusion efficiency of varicella-zoster virus (VZV) envelope glycoproteins was measured as a control (15). Cell-to-cell fusion was 10.2-fold more efficient with gB-, gH-, gL-, gQ1-, and gQ2-transfected effector cells than with mock-transfected effector cells (Fig. 3B). In the absence of gB, gH, gL, gQ1, or gQ2, no significant fusion activity was observed. gO of human cytomegalovirus (HCMV) and HHV-6 have been suggested to form a complex with gH and gL, with the complex being involved in HCMV entry (9, 27). However, transfection with HHV-6B gO did not affect cell-to-cell fusion induced by HHV-6B gB, gH, gL, gQ1, and gQ2 (data not shown). This is in agreement with the previous report that gO is not essential for HCMV cell-to-cell fusion (27). CD46-Ig also bound to HHV-6A (strain GS) gH, gL, gQ1, and gQ2 transfectants (data not shown), and cell-to-cell fusion was observed using HHV-6A envelope glycoproteins (Fig. 3A) (28). Furthermore, cell-to-cell fusion using either HHV-6A or -6B glycoproteins was inhibited by both anti-CD46 and anti-HHV-6A gB MAbs (clone 87-y-13), similar to reports in which syncytium formation by HHV-6A was abrogated by these MAbs (Fig. 4) (29, 30). These

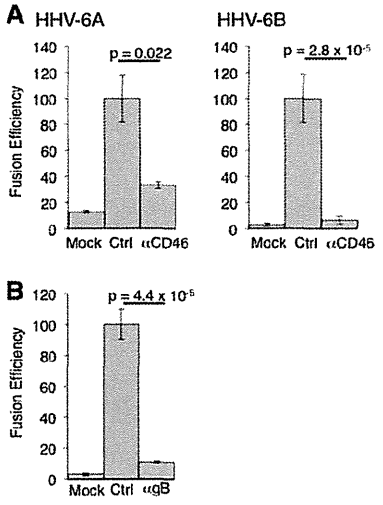

FIG 4 Effect of anti-CD46 and anti-gB MAbs on HHV-6-glycoprotein-mediated cell-to-cell fusion. (A) Cell-to-cell fusion efficiency mediated by HHV-6A and HHV-6B glycoproteins was measured in the presence of anti-CD46 MAb (M75), in the absence of anti-CD46 MAb (Ctrl), and in mock-transfected cells as described in the Fig. 3 legend. Fusion efficiency was calculated as follows: [(firefly luciferase activity/*Renilla* luciferase activity) × 100]/[(firefly luciferase activity/*Renilla* luciferase activity) in control cells]. (B) Cell-to-cell fusion efficiency mediated by HHV-6A glycoproteins was measured in the presence of anti-HHV-6A gB MAb (clone 87-y-13) and in the absence of anti-gB MAb (Ctrl) and in mock-transfected cells as described in the panel A legend. Error bars show the means ± SD of the results determined with quadruplicated samples. The statistical difference was determined by the Student's *t* test. A difference with $P < 0.05$ was considered statistically significant. Data are representative of at least three independent experiments.

results suggested that both HHV-6A and HHV-6B require gB, gH, gL, gQ1, and gQ2 for cell-to-cell fusion.

Cell-to-cell fusion assays were also done *in trans*; i.e., some cells were transfected only with plasmid(s) gB, gH/gL, and/or gQ1/gQ2 and other cells were transfected with plasmids expressing all the other glycoproteins. Little cell-to-cell fusion was observed in *in trans* fusion assays (data not shown). These results suggested that *cis* expression of HHV-6 gB, gH, gL, gQ1, and gQ2 is required for cell-to-cell fusion, unlike that of herpes simplex virus (HSV) and HCMV, in which all the envelope glycoproteins do not need to be expressed on the same cell (17, 31).

This is the first report showing that the HHV-6A and HHV-6B envelope glycoproteins gB, gH, gL, gQ1, and gQ2 are required for cell-to-cell fusion. Herpesviruses enter via two different pathways: (i) direct fusion of the viral envelope with the host cell membrane or (ii) endocytosis followed by fusion between the viral envelope and endosomal membranes (32). Since membrane fusion is needed for herpesvirus entry, our results are consistent with previous reports that anti-gB, -gH, and -gQ1 antibodies block HHV-6 infection (22–24, 33–36). Moreover, our results are also supported by an earlier report that gB and gH are required for polykaryocyte formation after virus infection of permissive cells in cell culture (29). Considering that gBs and gHs of other herpesviruses associate with their respective cellular receptors during viral entry and cell-to-cell fusion (15, 26, 37–41), HHV-6 gB may also mediate viral entry and cell-to-cell fusion by interaction with cellular receptors that are currently unknown in addition to the binding of the gH, gL, gQ1, and gQ2 complex to its receptor CD46. The virus-free HHV-6 fusion assay system developed in this study should help elucidate the HHV-6 entry mechanism.

ACKNOWLEDGMENTS

We thank M. Mastumoto and K. Shida for technical help, Y. Mori (Kobe University) for providing HHV-6A (GS)-infected cells and anti-gH and anti-gB (clone 87-y-13) MAbs, and Y. Matsuura (Osaka University) for providing pCAGT7 and pT7EMCluc.

This work was supported by a Grant-in-Aid for Scientific Research from the Ministry of Education, Science and Culture, Japan (T. Suenaga and H.A.) and in part by grants from the Takeda Science Foundation (T. Suenaga and H.A.).

REFERENCES

1. **Roizmann B, Desrosiers RC, Fleckenstein B, Lopez C, Minson AC, Studdert MJ.** 1992. The family Herpesviridae: an update. The Herpesvirus Study Group of the International Committee on Taxonomy of Viruses. Arch. Virol. 123:425–449.
2. **Aubin JT, Collandre H, Candotti D, Ingrand D, Rouzioux C, Burgard M, Richard S, Huraux JM, Agut H.** 1991. Several groups among human herpesvirus 6 strains can be distinguished by Southern blotting and polymerase chain reaction. J. Clin. Microbiol. 29:367–372.
3. **Campadelli-Fiume G, Guerrini S, Liu X, Foa-Tomasi L.** 1993. Monoclonal antibodies to glycoprotein B differentiate human herpesvirus 6 into two clusters, variants A and B. J. Gen. Virol. 74(Pt 10):2257–2262.
4. **Wyatt LS, Balachandran N, Frenkel N.** 1990. Variations in the replication and antigenic properties of human herpesvirus 6 strains. J. Infect. Dis. 162:852–857.
5. **Yamanishi K, Okuno T, Shiraki K, Takahashi M, Kondo T, Asano Y, Kurata T.** 1988. Identification of human herpesvirus-6 as a causal agent for exanthem subitum. Lancet i:1065–1067.
6. **Asano Y, Yoshikawa T, Suga S, Yazaki T, Kondo K, Yamanishi K.** 1990. Fatal fulminant hepatitis in an infant with human herpesvirus-6 infection. Lancet 335:862–863.
7. **Clark DA.** 2002. Human herpesvirus 6 and human herpesvirus 7: emerging pathogens in transplant patients. Int. J. Hematol. 76(Suppl 2):246–252.
8. **Maeki T, Mori Y.** 2012. Features of human herpesvirus-6A and -6B entry. Adv. Virol. 2012:384069. doi:10.1155/2012/384069.
9. **Mori Y, Akkapaiboon P, Yonemoto S, Koike M, Takemoto M, Sadaoka T, Sasamoto Y, Konishi S, Uchiyama Y, Yamanishi K.** 2004. Discovery of a second form of tripartite complex containing gH-gL of human herpesvirus 6 and observations on CD46. J. Virol. 78:4609–4616.
10. **Mori Y, Yang X, Akkapaiboon P, Okuno T, Yamanishi K.** 2003. Human herpesvirus 6 variant A glycoprotein H-glycoprotein L-glycoprotein Q complex associates with human CD46. J. Virol. 77:4992–4999.
11. **Santoro F, Kennedy PE, Locatelli G, Malnati MS, Berger EA, Lusso P.** 1999. CD46 is a cellular receptor for human herpesvirus 6. Cell 99:817–827.
12. **Chesnokova LS, Nishimura SL, Hutt-Fletcher LM.** 2009. Fusion of epithelial cells by Epstein-Barr virus proteins is triggered by binding of viral glycoproteins gHgL to integrins alphavbeta6 or alphavbeta8. Proc. Natl. Acad. Sci. U. S. A. 106:20464–20469.
13. **Haan KM, Lee SK, Longnecker R.** 2001. Different functional domains in the cytoplasmic tail of glycoprotein B are involved in Epstein-Barr virus-induced membrane fusion. Virology 290:106–114.
14. **Pertel PE.** 2002. Human herpesvirus 8 glycoprotein B (gB), gH, and gL can mediate cell fusion. J. Virol. 76:4390–4400.
15. **Suenaga T, Satoh T, Somboonthum P, Kawaguchi Y, Mori Y, Arase H.** 2010. Myelin-associated glycoprotein mediates membrane fusion and entry of neurotropic herpesviruses. Proc. Natl. Acad. Sci. U. S. A. 107:866–871.
16. **Turner A, Bruun B, Minson T, Browne H.** 1998. Glycoproteins gB, gD, and gHgL of herpes simplex virus type 1 are necessary and sufficient to mediate membrane fusion in a Cos cell transfection system. J. Virol. 72:873–875.
17. **Vanarsdall AL, Ryckman BJ, Chase MC, Johnson DC.** 2008. Human cytomegalovirus glycoproteins gB and gH/gL mediate epithelial cell-cell fusion when expressed either in cis or in trans. J. Virol. 82:11837–11850.
18. **Chowdary TK, Cairns TM, Atanasiu D, Cohen GH, Eisenberg RJ,**

Heldwein EE. 2010. Crystal structure of the conserved herpesvirus fusion regulator complex gH-gL. Nat. Struct. Mol. Biol. 17:882–888.
19. Eisenberg RJ, Atanasiu D, Cairns TM, Gallagher JR, Krummenacher C, Cohen GH. 2012. Herpes virus fusion and entry: a story with many characters. Viruses 4:800–832.
20. Heldwein EE, Lou H, Bender FC, Cohen GH, Eisenberg RJ, Harrison SC. 2006. Crystal structure of glycoprotein B from herpes simplex virus 1. Science 313:217–220.
21. Matsuura H, Kirschner AN, Longnecker R, Jardetzky TS. 2010. Crystal structure of the Epstein-Barr virus (EBV) glycoprotein H/glycoprotein L (gH/gL) complex. Proc. Natl. Acad. Sci. U. S. A. 107:22641–22646.
22. Foà-Tomasi L, Guerrini S, Huang T, Campadelli-Fiume G. 1992. Characterization of human herpesvirus-6(U1102) and (GS) gp112 and identification of the Z29-specified homolog. Virology 191:511–516.
23. Takeda K, Okuno T, Isegawa Y, Yamanishi K. 1996. Identification of a variant A-specific neutralizing epitope on glycoprotein B (gB) of human herpesvirus-6 (HHV-6). Virology 222:176–183.
24. Kawabata A, Oyaizu H, Maeki T, Tang H, Yamanishi K, Mori Y. 2011. Analysis of a neutralizing antibody for human herpesvirus 6B reveals a role for glycoprotein Q1 in viral entry. J. Virol. 85:12962–12971.
25. Tang H, Hayashi M, Maeki T, Yamanishi K, Mori Y. 2011. Human herpesvirus 6 glycoprotein complex formation is required for folding and trafficking of the gH/gL/gQ1/gQ2 complex and its cellular receptor binding. J. Virol. 85:11121–11130.
26. Satoh T, Arii J, Suenaga T, Wang J, Kogure A, Uehori J, Arase N, Shiratori I, Tanaka S, Kawaguchi Y, Spear PG, Lanier LL, Arase H. 2008. PILRalpha is a herpes simplex virus-1 entry coreceptor that associates with glycoprotein B. Cell 132:935–944.
27. Vanarsdall AL, Chase MC, Johnson DC. 2011. Human cytomegalovirus glycoprotein gO complexes with gH/gL, promoting interference with viral entry into human fibroblasts but not entry into epithelial cells. J. Virol. 85:11638–11645.
28. Akkapaiboon P, Mori Y, Sadaoka T, Yonemoto S, Yamanishi K. 2004. Intracellular processing of human herpesvirus 6 glycoproteins Q1 and Q2 into tetrameric complexes expressed on the viral envelope. J. Virol. 78: 7969–7983.
29. Mori Y, Seya T, Huang HL, Akkapaiboon P, Dhepakson P, Yamanishi K. 2002. Human herpesvirus 6 variant A but not variant B induces fusion from without in a variety of human cells through a human herpesvirus 6 entry receptor, CD46. J. Virol. 76:6750–6761.
30. Seya T, Hara T, Matsumoto M, Akedo H. 1990. Quantitative analysis of membrane cofactor protein (MCP) of complement. High expression of MCP on human leukemia cell lines, which is down-regulated during cell differentiation. J. Immunol. 145:238–245.
31. Atanasiu D, Saw WT, Cohen GH, Eisenberg RJ. 2010. Cascade of events governing cell-cell fusion induced by herpes simplex virus glycoproteins gD, gH/gL, and gB. J. Virol. 84:12292–12299.
32. Connolly SA, Jackson JO, Jardetzky TS, Longnecker R. 2011. Fusing structure and function: a structural view of the herpesvirus entry machinery. Nat. Rev. Microbiol. 9:369–381.
33. Liu DX, Gompels UA, Foa-Tomasi L, Campadelli-Fiume G. 1993. Human herpesvirus-6 glycoprotein H and L homologs are components of the gp100 complex and the gH external domain is the target for neutralizing monoclonal antibodies. Virology 197:12–22.
34. Okuno T, Sao H, Asada H, Shiraki K, Takahashi M, Yamanishi K. 1990. Analysis of a glycoprotein of human herpesvirus 6 (HHV-6) using monoclonal antibodies. Virology 176:625–628.
35. Qian G, Wood C, Chandran B. 1993. Identification and characterization of glycoprotein gH of human herpesvirus-6. Virology 194:380–386.
36. Takeda K, Haque M, Sunagawa T, Okuno T, Isegawa Y, Yamanishi K. 1997. Identification of a variant B-specific neutralizing epitope on glycoprotein H of human herpesvirus-6. J. Gen. Virol. 78(Pt 9):2171–2178.
37. Akula SM, Pramod NP, Wang FZ, Chandran B. 2002. Integrin alpha3beta1 (CD 49c/29) is a cellular receptor for Kaposi's sarcoma-associated herpesvirus (KSHV/HHV-8) entry into the target cells. Cell 108:407–419.
38. Arii J, Goto H, Suenaga T, Oyama M, Kozuka-Hata H, Imai T, Minowa A, Akashi H, Arase H, Kawaoka Y, Kawaguchi Y. 2010. Non-muscle myosin IIA is a functional entry receptor for herpes simplex virus-1. Nature 467:859–862.
39. Feire AL, Roy RM, Manley K, Compton T. 2010. The glycoprotein B disintegrin-like domain binds beta 1 integrin to mediate cytomegalovirus entry. J. Virol. 84:10026–10037.
40. Soroceanu L, Akhavan A, Cobbs CS. 2008. Platelet-derived growth factor-alpha receptor activation is required for human cytomegalovirus infection. Nature 455:391–395.
41. Wang X, Huong SM, Chiu ML, Raab-Traub N, Huang ES. 2003. Epidermal growth factor receptor is a cellular receptor for human cytomegalovirus. Nature 424:456–461.

JVI
Journals.ASM.org

Hepatitis C Virus Infection Induces Inflammatory Cytokines and Chemokines Mediated by the Cross Talk between Hepatocytes and Stellate Cells

Hironori Nishitsuji,[a] Kenji Funami,[b] Yuko Shimizu,[a] Saneyuki Ujino,[a] Kazuo Sugiyama,[c] Tsukasa Seya,[b] Hiroshi Takaku,[d] Kunitada Shimotohno[a]

Research Center for Hepatitis and Immunology, National Center for Global Health and Medicine, Ichikawa, Chiba, Japan[a]; Department of Microbiology and Immunology, Hokkaido University Graduate School of Medicine, Kita, Sapporo, Japan[b]; Center for Integrated Medical Research, Keio University, Shinjuku-ku, Tokyo, Japan[c]; Department of Life and Environmental Sciences, Chiba Institute of Technology, Narashino-shi, Chiba, Japan[d]

Inflammatory cytokines and chemokines play important roles in inflammation during viral infection. Hepatitis C virus (HCV) is a hepatotropic RNA virus that is closely associated with chronic liver inflammation, fibrosis, and hepatocellular carcinoma. During the progression of HCV-related diseases, hepatic stellate cells (HSCs) contribute to the inflammatory response triggered by HCV infection. However, the underlying molecular mechanisms that mediate HSC-induced chronic inflammation during HCV infection are not fully understood. By coculturing HSCs with HCV-infected hepatocytes *in vitro*, we found that HSCs stimulated HCV-infected hepatocytes, leading to the expression of proinflammatory cytokines and chemokines such as interleukin-6 (IL-6), IL-8, macrophage inflammatory protein 1α (MIP-1α), and MIP-1β. Moreover, we found that this effect was mediated by IL-1α, which was secreted by HSCs. HCV infection enhanced production of CCAAT/enhancer binding protein (C/EBP) β mRNA, and HSC-dependent IL-1α production contributed to the stimulation of C/EBPβ target cytokines and chemokines in HCV-infected hepatocytes. Consistent with this result, knockdown of mRNA for C/EBPβ in HCV-infected hepatocytes resulted in decreased production of cytokines and chemokines after the addition of HSC conditioned medium. Induction of cytokines and chemokines in hepatocytes by the HSC conditioned medium required a yet to be identified postentry event during productive HCV infection. The cross talk between HSCs and HCV-infected hepatocytes is a key feature of inflammation-mediated, HCV-related diseases.

Hepatitis C virus (HCV) can cause chronic liver disease, which can progress to fibrosis, cirrhosis, and hepatocellular carcinoma (HCC) (1). Clearance of HCV during the acute phase of infection is associated with a robust CD4 and CD8 T-cell response to multiple viral epitopes (2). However, clearance of HCV infection often fails because of an intermediate cytotoxic T-cell response that is unable to eliminate the infection but causes hepatocyte destruction. T-cell-mediated hepatocytotoxicity poses a high risk for progression to chronic liver inflammation and damage (3). During chronic HCV infection, chemokine-chemokine receptor interactions are particularly important for the recruitment of T cells to sites of inflammation in the liver. Liver-infiltrating lymphocytes in HCV patients exhibit increased expression of CXCR3 and CCR5 (4). Moreover, intrahepatic chemokines, such as RANTES, macrophage inflammatory protein 1α (MIP-1α), MIP-1β, and IP-10, are elevated in HCV patients (5), and intrahepatic proinflammatory cytokine levels are correlated with the severity of inflammation and liver fibrosis (6).

The induction of proinflammatory cytokines and chemokines is triggered by viral proteins and double-stranded RNA (dsRNA) from HCV. The HCV core protein induces inflammatory cytokines through the STAT3 signaling pathway (7). Retinoic acid-inducible gene I (RIG-I) and Toll-like receptor 3 (TLR-3) are cellular sensors that recognize HCV dsRNA, resulting in production of chemokines such as interleukin-8 (IL-8), RANTES, MIP-1α, and MIP-1β (8, 9). Recently, an alternative mechanism for HCV-induced inflammation was reported. It was demonstrated that NS5B, the viral RNA-dependent RNA polymerase (RdRp), catalyzes production of small RNA species that trigger an innate immune response, leading to the production of both interferon (IFN) and inflammatory cytokines (10).

Hepatic stellate cells (HSCs) represent 5 to 8% of the total human liver cells and reside in the Disse space (11). Activation or transdifferentiation of HSCs is regulated by growth factors, including transforming growth factor β (TGF-β), which are associated with pathological conditions such as liver injury, cirrhosis, and cancer (11, 12). During liver injury, quiescent HSCs become activated and convert into highly proliferative, myofibroblast-like cells, which produce inflammatory and fibrogenic mediators (13). In a human hepatoma model, the cross talk between tumor hepatocytes and activated HSCs induced an inflammatory response, and the amounts of cytokines and chemokines associated with hepatocyte-HSC cross talk correlated to HCC progression (14).

Although direct induction of liver inflammation by HCV infection through cellular sensors or HCV proteins is well documented, little is known about the mechanisms governing the proinflammatory cytokines and chemokines that are produced during the interactions between HCV-infected hepatocytes and HSCs. Here, we show that HSCs can act as an inflammatory mediator to HCV-infected cells. Infection of hepatocytes with HCV

Received 9 April 2013 Accepted 9 May 2013
Published ahead of print 15 May 2013
Address correspondence to Hironori Nishitsuji, lbnishitsuji@hospk.ncgm.go.jp, or Kunitada Shimotohno, lbshimotohno@hospk.ncgm.go.jp.

doi:10.1128/JVI.00974-13

resulted in increased CCAAT/enhancer binding protein (C/EBPβ) production. Conditioned medium (CM) from HSCs induced hepatocyte production of inflammatory cytokines and chemokines, such as IL-6, IL-8, and MIP-1β, which are potential targets of C/EBPβ. Stimulation of these cytokines and chemokines in HCV-infected cells by HSC CM was suppressed by knockdown of mRNA for C/EBPβ. From the chemokines secreted by HSCs, IL-1α was identified as the inducer of MIP-1β. These results suggest HSCs may contribute to virus infection-associated liver inflammation through cross talk with HCV-infected hepatocytes.

MATERIALS AND METHODS

Cells. LX2 cells (kindly provided by S. Friedman), NP-2-CCR5 cells (kindly provided by T. Hoshino), and Huh7.5 cells (kindly provided by C. Rice) were cultured in Dulbecco's modified Eagle's medium (DMEM) (Invitrogen) supplemented with 10% fetal bovine serum (FBS), 100 μg/ml penicillin and streptomycin, and 100 U/ml nonessential amino acids (Invitrogen). To maintain the quality of the cells, stored frozen stocks were thawed every 3 months and used in the experiments.

Plasmids. DNA fragments encoding each of the HCV nonstructural proteins were generated from a full-length cDNA clone of JFH1 by PCR. The fragments were cloned into pCAG-GS/N-Flag, in which the sequence encoding a Flag tag is inserted at the 5′ terminus of the cloning site of pCAG-GS.

Virus. Infectious HCV in cell culture (HCVcc) was produced by transfection of Huh7.5 cells with *in vitro*-transcribed RNA derived from JFH1 (kindly provided by T. Wakita) or TNS2J1 (the chimeric HCV genome containing HCV-1b in the structure region and JFH1 non-structural-protein-coding regions). UV-irradiated JFH1 was prepared by irradiation with a UV lamp of 254-nm wavelength at a distance of 6 cm for 1 min.

HCV infection. Huh7.5 cells were infected with JFH1 at a multiplicity of infection (MOI) of 5. Under this condition, 80 to 90% of the cells became positive for HCV core protein after 3 days.

Preparation of conditioned medium from Huh7.5 or LX2 cells. Huh7.5 or LX2 cells (1×10^6) were seeded in 10 ml of medium in a 100-mm dish for 3 days. Supernatants were collected and filtered through 0.45-μm-pore-size filters.

Chemotaxis of NP-2-CCR5 cells. A 60-fold concentration of Huh7.5 or LX2 CM was generated by tapping in a filter membrane that cut off the 100-kDa-molecular-mass marker protein (100,000-molecular-weight-cutoff filter) and was used for experimental stimulations. Huh7.5 or JFH1-infected Huh7.5 cells (Huh7.5/JFH1 cells) were treated with each concentrated CM. After 24 h of treatment, the medium was changed to serum-free DMEM for 24 h and then used for chemotaxis assays. Chemotaxis of NP-2-CCR5 cells was measured in a 48-well chemotaxis chamber (Neuro Probe). The chamber consisted of a 48-well upper chamber and a 48-well lower chamber separated by a polycarbonate filter (pore size, 8 μm) coated with rat tail collagen. The lower wells were filled with each conditioned medium. The NP-2-CCR5 cells were washed and suspended in serum-free DMEM in the absence or presence of 0.1 nM maraviroc and then divided in the upper wells (5,000 cells per well). After incubation at 37°C for 180 min, the cells that had migrated into the lower well of the 48-well chemotaxis chamber were counted by Diff-Quik staining.

Quantitative RT-PCR. Total RNA was extracted from cells using RNeasy minikits (Qiagen), and cDNA was prepared with SuperscriptIII (Invitrogen) using oligo(dT) primers. Quantitative real-time PCR (qRT-PCR) was performed with Fast SYBR green master mix (Applied Biosystems), and fluorescent signals were analyzed with the Fast RT-PCR system (Applied Biosystems). The PCR primer pairs are described in Table 1.

siRNA transfection. Small interfering RNA (siRNA) was transfected using Lipofectamine RNAiMAX reagent (Invitrogen) according to the manufacturer's protocol. The duplex nucleotides of siRNA specific to the mRNA for C/EBPβ (5′-GAAGAAACGUCUAUGUGUA-3′) and the Mission siRNA universal negative control were purchased from Sigma. Synthetic siRNA specific to mRNA for IL-1 receptor-associated kinase 1 (IRAK1) (5′-CCCGGGCAAUUCAGUUUCUACAUCA-3′) and the Stealth RNA interference (RNAi) negative control duplex were purchased from Invitrogen.

TABLE 1 Real-time PCR primers

Primer	Sequence (5′–3′)
CXCL1-F	GCAGGGAATTCACCCCAAGAAC
CXCL1-R	CTATGGGGGATGCAGGATTGAG
CXCL2-F	CCAACTGACCAGAAGGAAGGAG
CXCL2-R	ATGGCCTCCAGGTCATCATCAG
CXCL5-F	TGAGAGAGCTGCGTTGCGTTTG
CXCL5-R	TTCCTTCCCGTTCTTCAGGGAG
CXCL6-F	CTGCGTTGCACTTGTTTACGCG
CXCL6-R	GGGTCCAGACAAACTTGCTTCC
IL-1alpha-F	AGCTATGGCCCACTCCATGAAG
IL-1alpha-R	ACATTAGGCGCAATCCAGGTGG
IL-6-F	CCCCCAGGAGAAGATTCCAAAG
IL-6-R	TTCTGCCAGTGCCTCTTTGCTG
IL-7-F	ATTCCGTGCTGCTCGCAAGTTG
IL-7-R	AACCTGGCCAGTGCAGTTCAAC
IL-8-F	CTGTTAAATCTGGCAACCCTAGTCT
IL-8-R	CAAGGCACAGTGGAACAAGGA
MIP-1alpha-F	GCTGACTACTTTGAGACGAGC
MIP-1alpha-R	CCAGTCCATAGAAGAGGTAGC
MIP-1beta-F	CAGCGCTCTCAGCACCAATGG
MIP-1beta-R	GATCAGCACAGACTTGCTTGCTTC
C/EBP-beta-F	CTCGCAGGTCAAGAGCAAG
C/EBP-beta-R	GACAGCTGCTCCACCTTCTT
Collagen-F	AACATGACCAAAAACCAAAAGTG
Collagen-R	CATTGTTTCCTGTGTCTTCTGG
IL-1R-F	CCTGTCTTATGGCGTTGCAGGC
IL-1R-R	AGTGCCCTGGGCTGCTATTGAC

Cytokine antibody array. LX2 cells (1×10^6) were seeded in 10 ml of medium in a 100-mm dish for 2 days. The supernatant was then changed to 0.2% FBS-DMEM. Two days after incubation, the supernatants were collected and then concentrated by using a 100,000-molecular-weight-cutoff filter. The trapped and flowthrough fractions were dialyzed with phosphate-buffered saline (PBS) for 18 h. The amount of protein in each fraction was determined using a bicinchoninate protein assay kit (Nacalai Tesque). Three milligrams of each fraction was subjected to the cytokine antibody array.

The expression levels of 507 human proteins in the trap and flowthrough fractions from the LX2 cells were determined using biotin label-based human antibody array I (Raybiotech) according to the manufacturer's protocol.

RESULTS

LX2 cells induce MIP-1β expression in JFH1-infected Huh7.5 cells. Our preliminary results indicated that coculturing human hepatic stellate cells (HSCs) with HCV-infected cells stimulated the expression of MIP-1β, which was found to be one of most upregulated chemokines. Here, we focused on its role as a marker of inflammation.

To investigate whether human HSCs play a role in the proinflammatory response of HCV-infected cells, JFH1-infected Huh7.5 cells were cocultured with LX2 cells, which are an HSC line generated by spontaneous immortalization in low-serum conditions (15). The expression of MIP-1β mRNA was then determined by qRT-PCR. Compared to the level in uninfected Huh7.5 cells, HCV infection induced a low level of MIP-1β expression (Fig. 1A, Huh7.5/JFH1). Moreover, MIP-1β expression

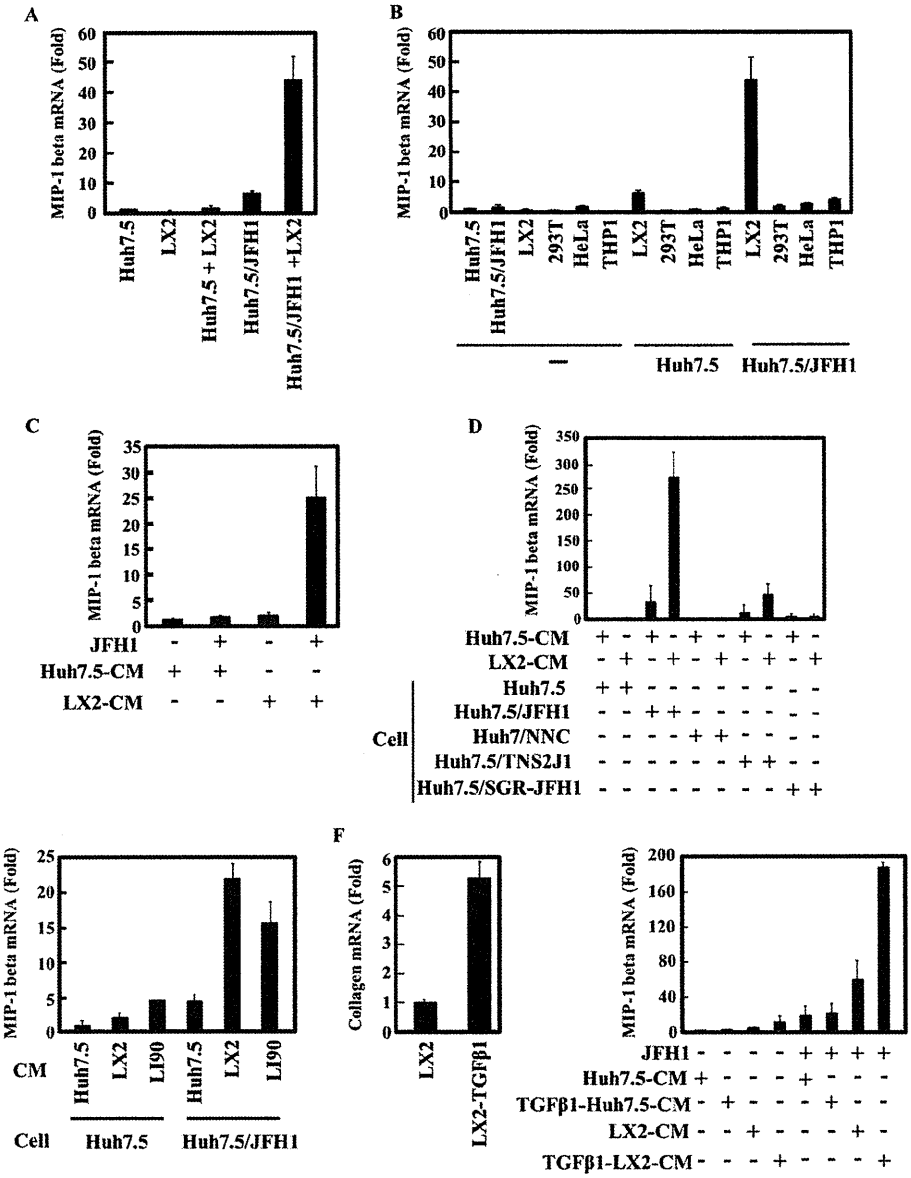

FIG 1 Conditioned medium from LX2 induces MIP-1β expression in JFH1-infected Huh7.5 cells. (A) Huh7.5 cells (1×10^5 cells) and JFH1-infected Huh7.5 (Huh7.5/JFH1) cells (1×10^5 cells) were cultured alone or in the presence of LX2 cells (1×10^5 cells) for 24 h. The level of MIP-1β was measured by qRT-PCR. Quantitative analysis of the PCR data was performed using the $2^{-\Delta\Delta CT}$ method, and glyceraldehyde-3-phosphate dehydrogenase (GAPDH) C_T values were used for normalization. The fold changes are relative to values for Huh7.5 cells. (B) Huh7.5 cells and JFH1-infected Huh7.5 cells (Huh7.5/JFH1) were cultured alone or in the presence of LX2, 293T, HeLa, or THP-1 cells for 24 h. The expression level of MIP-1β was measured by qRT-PCR as described for panel A. (C) Huh7.5 cells and JFH1-infected Huh7.5 cells were treated with conditioned medium from Huh7.5 (Huh7.5 CM) or LX2 (LX2 CM) cells for 24 h. The expression level of MIP-1β was measured by qRT-PCR as described for panel A. (D) Huh7.5, JFH1-infected Huh7.5 (Huh7.5/JFH1), Huh7/NNC, Huh7.5/TNS2J1, and Huh7.5/SGR-JFH1 cells were treated with CM from Huh7.5 or LX2 cells for 24 h. The expression level of MIP-1β was measured by qRT-PCR as described for panel A. (E) Huh7.5 and JFH1-infected Huh7.5 (Huh7.5/JFH1) cells were treated with Huh7.5 CM, LX2 CM, or LI90 CM for 24 h. The expression level of MIP-1β was measured by qRT-PCR as described for panel A. (F) LX2 cells were treated with 2.5 ng/ml TGF-β1 for 24 h, and then the level of collagen mRNA in these cells was determined by qRT-PCR (left). Huh7.5 or JFH1-infected Huh7.5 cells were treated with LX2 CM or TGF-β1-stimulated LX2 CM for 24 h. The expression level of MIP-1β was measured by qRT-PCR as described for panel A (right). The results are representative of three independent experiments, and the error bars represent the standard deviation of the means.

was significantly enhanced in JFH1-infected Huh7.5 cells after they were cocultured with LX2 cells (Fig. 1A, Huh7.5/JFH1+LX2). Importantly, MIP-1β expression was undetectable or very low in LX2 cells alone or in uninfected Huh7.5 cells cocultured with LX2 (Fig. 1A, LX2 and Huh7.5+LX2). Interestingly, increased MIP-1β expression in JFH1-infected Huh7.5 cells was specifically induced by cocultivation with LX2 cells. Cocultivation with other cell lines, such as 293T, HeLa, and THP-1, had no effect on MIP-1β expression in JFH1-infected Huh7.5 cells (Fig. 1B). These results suggest that Huh7.5 cells produce MIP-1β in re-

sponse to HCV infection and that LX2 cells increase MIP-1β expression in HCV-infected Huh7.5 cells.

We next determined whether MIP-1β induction by LX2 cells in HCV-infected cells was mediated by a secreted soluble factor(s). Huh7.5 and JFH1-infected Huh7.5 cells were treated with conditioned medium (CM) from Huh7.5 or LX2 cells (Fig. 1C). As expected, Huh7.5 cells had no response to Huh7.5 CM or LX2 CM. However, we observed that LX2 CM, but not Huh7.5 CM, stimulated MIP-1β expression in JFH1-infected Huh7.5 cells. These results indicated that LX2 cells secrete a factor that stimulates MIP-1β expression.

To address whether MIP-1β stimulation after culturing with LX2 CM is dependent on HCV genotype or on the maintenance of the HCV replicon in cells, we used Huh7.5 cells that carry different types of the HCV genome. Huh7/NNC cells are Huh7 cells that contain the noninfectious full HCV genotype 1b, Huh7.5/SGR-JFH1 cells contain the subgenome replicon of JFH1, and Huh7.5/TNS2J1 cells have the infectious chimeric HCV genome, which consists of an HCV-1b-derived sequence in the structural-protein-coding region and a JFH-derived sequence in nonstructural-protein-coding region (Fig. 1D). In Huh7.5/TNS2J1 cells, MIP-1β expression was significantly induced by LX2 CM (47-fold), though there was a lower level of expression than what was observed in JFH1-infected cells (272-fold). By contrast, NNC and SGR-JFH1 had no effect on MIP-1β expression. These results demonstrate that LX2 CM-induced stimulation of MIP-1β expression may require a productive HCV infection (see also Fig. 6).

Because LX2 cells are a human hepatic stellate cell line that was established by immortalization, we confirmed our findings by using another human hepatic stellate cell line, LI90, which was derived from a human mesenchymal liver tumor (16). When uninfected or JFH1-infected Huh7.5 cells were treated with LI90 CM, MIP-1β expression was increased only in the JFH1-infected Huh7.5 cells. These results are similar to those found after addition of LX2 CM to JFH1-infected Huh7.5 cells (Fig. 1E).

Activated hepatic stellate cells play a critical role in inflammation, yet the functional impact they have on hepatocytes has not yet been determined. Therefore, we evaluated whether the activation of LX2 cells affects the expression of MIP-1β in JFH1-infected Huh7.5 cells. LX2 cells were treated with TGF-β1, and the mRNA expression of the collagen gene, a marker of HSC activation, was measured (Fig. 1F, left). LX2 CM from activated cells significantly enhanced MIP-1β expression in JFH1-infected Huh7.5 cells but not in uninfected Huh7.5 cells, compared to the increase with nonactivated LX2 CM (Fig. 1F, right). In parallel experiments, TGF-β1-treated Huh7.5 CM did not affect MIP-1β expression in Huh7.5 or JFH1-infected Huh7.5 cells.

The supernatant from JFH1-infected Huh7.5 cells cultured with LX2 CM induces migration of NP-2-CCR5 cells. MIP-1β is a physiological ligand for the CCR5 receptor. To test whether MIP-1β produced by HCV-infected hepatocytes that have been cultured with LX2 CM has this activity, we performed a chemotactic assay using NP-2-CCR5 cells, a human glioma-derived cell line expressing CCR5 on its cell surface (Fig. 2). The treatment of NP-2-CCR5 cells with supernatant from LX2 CM-stimulated JFH1-infected Huh7.5 cells increased their migration by 2-fold compared to treatment with supernatant from uninfected Huh7.5 cells treated with LX2 CM. This increase in NP-2-CCR5 cell migration was blocked with maraviroc (a CCR5 antagonist) treatment. These results indicated that LX2 CM induces secretion of a physiologically functional MIP-1β by JFH1-infected Huh7.5 cells.

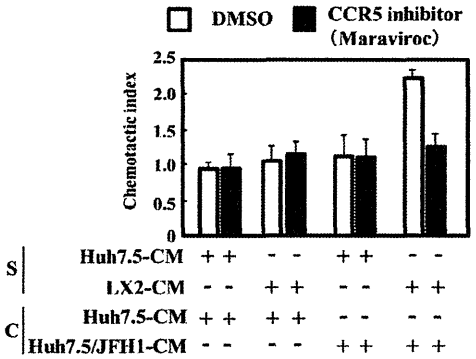

FIG 2 Conditioned medium from JFH1-infected Huh7.5 cells treated with LX2-conditioned medium induces chemotaxis of NP-2-CCR5 cells. Huh7.5 CM or LX2 CM was concentrated 60-fold using a 100,000-molecular-weight-cutoff membrane filter. Huh7.5 and Huh7.5/JFH1 cells were treated with each concentrated medium (S). After 24 h of treatment, the medium was changed to serum free DMEM for 24 h. The chemotactic activity of each conditioned medium (C) was determined by using 5 nM maraviroc (CCR5 inhibitor) and NP-2-CCR5 cells, as described in Materials and Methods. The results are representative of three independent experiments, and the error bars represent the standard deviations of the means. DMSO, dimethyl sulfoxide.

Identification of the factor in LX2 CM responsible for MIP-1β stimulation. We first fractionated culture medium of Huh7.5 or LX2 cells using a membrane filter which cut off the 100-kDa-molecular-mass marker protein and then collected the trapped and flowthrough fractions. As expected, MIP-1β expression in uninfected Huh7.5 or JFH1-infected Huh7.5 cells did not increase after treatment with the trap or the flowthrough fraction of the Huh7.5 CM (Fig. 3A). By contrast, the trap fraction of LX2 CM enhanced MIP-1β expression in JFH1-infected Huh7.5 cells, suggesting that the stimulator in the LX2 CM was enriched in the 100-kDa-molecular-mass-cutoff filter. To further analyze the trap fraction of LX2 CM, we created a cytokine antibody array (Fig. 3B). By analyzing 507 cytokines and chemokines in the array, we found four candidates (TSG-14, monocyte chemoattractant protein 2 [MCP-2], MCP-3, and IL-1α), which were more concentrated by the 100-kDa-molecular-mass-cutoff filter than by the flowthrough fraction of LX2 CM (Fig. 3B, compare 100K-Flow through to 100K-Trap). We tested the effects of these candidates on stimulation of MIP-1β expression (Fig. 4A). Although recombinant TSG-14, MCP-2, or MCP-3 did not stimulate MIP-1β expression in Huh7.5 cells or JFH1-infected cells, recombinant IL-1α induced MIP-1β expression in only JFH1-infected Huh7.5 cells. This effect was dose dependent (Fig. 4B). To evaluate whether IL-1α is required for MIP-1β stimulation in JFH1-infected Huh7.5 cells by LX2 CM, we used a neutralizing antibody against IL-1α and the IL-1 receptor antagonist. LX2 CM stimulated MIP-1β expression in JFH1-infected Huh7.5 cells, whereas anti-IL-1α and the IL-1 receptor antagonist (IL-1RA) blocked MIP-1β stimulation (Fig. 4C). Additionally, the neutralizing antibody against IL-1β had no effect (data not shown). It is not clear why IL-1α of about 30 kDa was concentrated into the trap fraction. However, it is likely that IL-1α is formed at a large mass with other proteins in the culture medium to be contained. Moreover, knockdown of IRAK1, which is essential for the downstream sig-

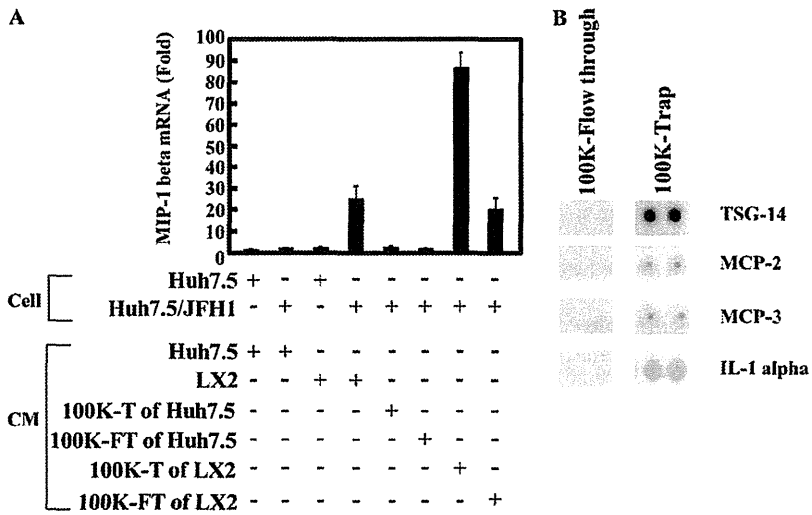

FIG 3 Identification of a factor(s) in the LX2 conditioned medium that is responsible for induction of MIP-1β expression. (A) Huh7.5 CM or LX2 CM was concentrated using a 100,000-molecular-weight-cutoff membrane filter. Huh7.5 and JFH1-infected Huh7.5 (Huh7.5/JFH1) cells were treated with each unconcentrated conditioned medium, with the flowthrough fraction (100K-FT), or with the trap fraction (100K-T). The MIP-1β expression level was analyzed by qRT-PCR as described for Fig. 1A. (B) LX2 CM was concentrated using a 100,000-molecular-weight-cutoff membrane filter. A cytokine antibody array (RayBiotech) was used for the simultaneous detection of 507 inflammatory factors. The antibody-coated membrane was incubated with the trap fraction (100K-Trap) or with the flowthrough fraction (100K-Flow through). Representative spots (TSG-14, MCP-1, MCP-3, and IL-1α) are shown.

nal of IL-1R, impaired the response to LX2 CM (Fig. 4D). These results suggest that IL-1α contributes to stimulation of MIP-1β expression by LX2 CM and that JFH1-infected Huh7.5 cells are highly sensitive to IL-1α. Furthermore, considering the molecular weight of IL-1α, it is possible that an unknown amount of IL-1α, undetectable by the cytokine antibody array, passed through the filter, which caused activation of MIP-1b by the 100,000-molecular-weight-cutoff flowthrough fraction. Alternatively, a factor(s) other than IL-1α in the 100,000-molecular-weight-cutoff flowthrough fraction might have been responsible for the activation.

The transcription factor C/EBPβ mediates LX2 CM-stimulated MIP-1β production. IL-1 is one of the most important proinflammatory cytokines and binds to the cell surface IL-1 type I receptor to activate downstream signaling pathways such as IKK–NF-κB, extracellular signal-regulated kinase (ERK), Jun N-terminal protein kinase (JNK), p38, and C/EBPβ. Moreover, the MIP-1β promoter contains a C/EBPβ motif located between bp −222 and −100, and the C/EBPβ promoter is required for a functional response to IL-1β in human chondrocytes (17). To evaluate whether LX2 CM-stimulated MIP-1β expression involves C/EBPβ stimulation, the level of C/EBPβ mRNA was measured in uninfected and HCV-infected cells. C/EBPβ expression was higher in Huh7.5/JFH1 and Huh7.5/TNS2J1 cells than in Huh7.5, Huh7/NNC, and Huh7.5/SGR-JFH1 cells (Fig. 5A). This result correlates with MIP-1β stimulation shown in Fig. 1D. Additionally, LX2 CM induced low levels of C/EBPβ expression in Huh7.5/JFH1 and Huh7.5/TNS2J1 cells; induction was likely caused by IL-1α (Fig. 5A). To further confirm that the enhancement of MIP-1β expression is mediated by C/EBPβ, we performed experiments where uninfected or JFH1-infected Huh7.5 cells were transduced with either a control or a C/EBPβ-specific siRNA and then treated with Huh7.5 CM or LX2 CM. Quantitative RT-PCR analysis demonstrated that the siRNAs targeting C/EBPβ significantly suppressed endogenous C/EBPβ expression (Fig. 5B). Depletion of C/EBPβ significantly reduced the MIP-1β expression stimulated by LX2 CM in JFH1-infected Huh7.5 cells. Residual stimulation of MIP-1β seems to be attributable to imperfect knockdown of C/EBPβ (70 to 80%). However, currently we cannot rule out the possibility of the involvement of other transcription factor(s) in the activation of MIP-1β expression. Furthermore, cytokines (IL-6, IL-8, CXCL2, CXCL1, MIP-1β, and MIP-1α) that were enhanced by C/EBPβ expression were upregulated by LX2 CM only in JFH1-infected Huh7.5 cells (Fig. 5D). There was no induction of C/EBPβ-independent cytokines (IL-7, CXCL6, CXCL5, IL-1α, and IL-1R) after the addition of LX2 CM. None of these cytokines were induced by LX2 CM in uninfected Huh7.5 cells. These data indicate that HCV stimulates C/EBPβ expression, which confers upon HCV-infected Huh7.5 cells the ability to produce proinflammatory cytokines in response to LX2 CM.

Early steps of the HCV life cycle trigger MIP-1β stimulation by LX2 CM. We observed that Huh7.5/TNS2J1 and Huh7.5/JFH1 cells, but not Huh7/NNC or Huh7.5/SGR-JFH1 cells, could respond to LX2 CM (Fig. 1D), suggesting that the production of infectious HCV is required for MIP-1β induction. However, it remains to be determined whether infectious HCV particles actually induce MIP-1β expression in the presence of LX2 CM. To address this question, we used JFH1-CL3B, which is a virus that is defective in the production of virus particles because of mutations in domain III of NS5A; however, the self-replication ability of its genome is normal (18). As shown in Fig. 6A, JFH1-CL3B genome-bearing Huh7.5 cells responded to neither Huh7.5 CM nor LX2 CM. These data suggest that productive infection of HCV is an essential event for MIP-1β induction. To characterize the mechanism that mediates LX2 CM-stimulated MIP-1β induction in HCV-infected cells, we studied the temporal kinetics of MIP-1β expression. In JFH1-infected Huh7.5 cells, MIP-1β expression did not increase in the first 2 h after infection but it started to increase after 4 h in the presence of LX2 CM (Fig. 6B). Furthermore,